

Geological Society of America Bulletin, in press

Paleo-fluid flow and deformation in the Aztec Sandstone at the Valley of Fire, Nevada—Evidence for the coupling of hydrogeologic, diagenetic, and tectonic processes

Peter Eichhubl, W. Lansing Taylor*, David D. Pollard, and Atilla Aydin

Department of Geological and Environmental Sciences, Stanford University, Stanford, CA 94305-2115

* Present address: Anadarko Petroleum Corporation, 1201 Lake Robbins Drive, The Woodlands, TX 77380

e-mail: eichhubl@pangea.stanford.edu

ABSTRACT

Paleo-fluid flow conditions are reconstructed for an exhumed faulted and fractured sandstone aquifer, the Jurassic Aztec Sandstone at Valley of Fire, Nevada. This reconstruction is based on detailed mapping of multicolored alteration patterns that resulted from syndepositional reddening of the eolian sandstone and repeated episodes of dissolution, mobilization, and re-precipitation of iron oxide and hydroxide. A first stage of bleaching and local redeposition of hematite is attributed to upward migration of reducing basinal fluid during and subsequent to Late Cretaceous Sevier thrusting and foreland deposition of clastic sediments. A second stage of bleaching and iron remobilization, precipitating predominantly goethite and minor iron sulfates, occurred during Miocene strike-slip faulting associated with Basin and Range tectonics. This second stage is explained by mixing of reducing sulfide-rich basinal fluid with meteoric water entering the aquifer. The distribution of alteration patterns indicates that regional-scale fluid migration pathways were controlled by stratigraphic contacts and by thrust faults, whereas the outcrop-scale focusing of flow was controlled by structural heterogeneities such as joints, joint-based faults, and deformation bands as well as the sedimentary architecture. The complex interaction of structural heterogeneities with alteration is consistent with their measured hydraulic properties demonstrating the significance of structural heterogeneities for focused fluid flow in a porous sandstone aquifer.

Keywords: fluid flow, sandstone, hematite, diagenesis, deformation, thrust.

INTRODUCTION

Understanding the spatial and temporal distribution of fluid flow in the subsurface is of fundamental importance to the successful management of groundwater and hydrocarbon resources. In addition, the interaction of formation fluids with the hydrosphere and atmosphere is of increasing environmental concern (Moore, 1999). Of particular significance to these processes are the effects of structural heterogeneities such as faults and fractures in controlling diagenetic precipitation and dissolution and the combined effects of deformation and diagenesis in controlling the fluid migration pathways and their permeability.

This study followed a paleo-hydrologic approach to investigate these effects in an exhumed faulted and fractured sandstone reservoir and aquifer. This investigative approach reconstructs the spatial and temporal variation of fluid flow based on crosscutting relations between structures and diagenetic features that are observable in outcrop or with analytical techniques. Diagenetic features that are indicative of past fluid flow include alteration boundaries that, in some cases, allow inference of the direction of fluid flow. Outcrop analog studies of paleo-flow systems are particularly useful in providing a three-dimensional view of the influence

of structures on fluid flow at scales ranging from microscopic to regional. In addition, outcrop-analog studies can assess temporal variations in flow regimes over geologic time scales.

We investigated paleo-fluid flow in the Jurassic Aztec Sandstone at Valley of Fire State Park in southeastern Nevada. The Aztec Sandstone has undergone multiple episodes of deformation and diagenetic alteration including the precipitation, dissolution, and remobilization of iron oxides and hydroxides. These oxidation and reduction reactions provide a record of paleo-fluid flow that is readily identifiable in the field allowing the spatial reconstruction of flow migration pathways and flow direction. Based on cross-cutting relations with structural features, we demonstrate that the timing and focusing of fluid flow across this sandstone unit was strongly influenced by deformation and tectonic processes. This paper emphasizes map-scale processes. The relationships between alteration and deformation on the outcrop scale and the in-situ hydraulic properties of structural features were described earlier in separate publications stemming from this and related research efforts (Myers, 1999; Taylor et al., 1999; Taylor and Pollard, 2000; Jourde et al., 2002; Flodin et al., 2004).

GEOLOGIC SETTING

Valley of Fire State Park is situated 60 km northeast of Las Vegas, Nevada (Fig. 1) within the Basin and Range physiographic province, 50 km west of the western edge of the Colorado Plateau. The park derives its name from the multicolored sandstone formations that range in hue from orange-red to purple, yellow, and white and that are part of the 1400 m thick Upper Triassic and Jurassic Aztec Sandstone (Bohannon, 1977, 1983), an eolian sediment deposited in a back-arc setting (Marzolf, 1983, 1990). The Aztec Sandstone is part of a Mesozoic clastic sequence that overlies Upper Paleozoic carbonates and shale (Bohannon, 1983). Triassic redbeds of the Moenkopi, Chinle, and Moenave formations, with a combined thickness of up to 2100 m (Bohannon, 1977), are composed of sand-, silt-, and mudstone with evaporite layers (Marzolf, 1990). The Aztec Sandstone is unconformably overlain, with a discordance of locally up to 10°, by a distinctive conglomerate that forms the basal member of the Cretaceous Willow Tank Formation. The Willow Tank Formation, composed of predominantly mudstone, and the overlying sandstone and conglomerate layers of the Baseline Sandstone have a combined thickness of about 1300 m (Bohannon, 1977). These units are interpreted as syn-orogenic foreland deposits of the eastward-directed Cretaceous Sevier thrust sheets (Bohannon, 1983). The basal conglomerate of the Willow Tank Formation includes locally derived red Aztec sandstone components (Longwell, 1949) among far-traveled quartzite components indicative of partial exhumation and erosion of the Aztec Sandstone subsequent to its deposition (Bohannon, 1983).

The Willow Tank Formation and lower portions of the Cretaceous Baseline Sandstone are overthrust by Aztec Sandstone of the Willow Tank thrust sheet (Figs. 1 and 2), the lowest of the Sevier thrust sheets in the study area (Longwell, 1949; Bohannon, 1983). Tearfault Mesa in the northern part of Figure 1 forms a klippe of the Willow Tank thrust sheet. Cretaceous strata are steepened and locally overturned along the eastern margin of this klippe (Longwell, 1949) indicating that the eastern edge of the klippe represents the leading edge of the thrust sheet. Upper portions of the Baseline Sandstone are deposited on top of the Willow Tank thrust sheet constraining the age of thrusting to Late Cretaceous (Maastrichtian) (Longwell, 1949; Bohannon, 1983).

With a hiatus during Paleogene times, deposition of clastic units continued conformably during Oligocene to Pliocene times (Bohannon, 1983). A ~25° angular unconformity at the base of the Upper Miocene (10-4 Ma) Muddy Creek Formation (Bohannon et al., 1993) constrains the time of tilting of the Aztec Sandstone, presently dipping 20-30° northeast. The Muddy Creek Formation, in turn, dips 5-8° northeast indicating continued tilting throughout the Late Miocene. The Aztec Sandstone and overlying Cretaceous strata are folded into a gentle NE-plunging syncline referred to as Overton syncline by Carpenter and Carpenter (1994) (Fig. 1).

DEFORMATION

Deformation structures in the Aztec Sandstone include deformation bands, joints and sheared joints, and faults that are composed of deformation bands, slip surfaces, sheared joints, and breccia zones.

Deformation bands are tabular features of localized deformation that are frequently more resistant to erosion and thus observed on the outcrop as ridges ranging in thickness from 1 mm to 10 cm, with a typical width of about 1 cm (Antonellini & Aydin, 1994). At Valley of Fire, Hill (1989) distinguished three earlier sets of deformation bands, striking northwest, north-northwest, and north-northeast, that are characterized by predominant band-parallel compaction. Following Mollema and Antonellini (1996) we refer to these deformation bands as compaction bands. Repeated mutual cross-cutting suggests that these three sets formed concurrently. The three sets of compaction bands are cross-cut by three sets of deformation bands (Flodin and Aydin, 2004) that exhibit macroscopic shear offsets and are therefore referred to as shear bands. One set of shear bands, with slip ranging from 1-3 cm, parallels depositional boundaries of the cross-bedded strata (Hill, 1989). The other two sets of shear bands usually occur as subvertical zones of multiple shear bands and associated slip surfaces, with slip on the order of decimeters (Flodin and Aydin, 2004). The top-to-the-east sense of shear of the bed-parallel shear bands is kinematically consistent with Sevier thrusting suggesting that these shear bands formed concurrently with thrusting.

Taylor et al. (1999) distinguished four sets of joints in the Aztec Sandstone. The first set is composed of parallel vertical joints that strike roughly north-south. This set is locally replaced by two sets of joints that also strike north-south but form two intersecting sets with an acute angle of about 30°. Joints of the fourth set are slightly sinuous and do not show a strong preferred orientation, but may favor a roughly east-west orientation. Joints have been observed to consistently crosscut compaction and shear bands and are thus interpreted to form after deformation bands and concurrently with, and possibly also prior to, strike-slip faulting (Myers, 1999; Flodin and Aydin, 2004).

Two sets of oblique-slip faults with predominant strike-slip and lesser normal-slip components occur as two sets, a left-lateral fault set striking NNE and a right-lateral set striking NW (Myers, 1999; Flodin and Aydin, 2004). (Fig. 1). The NNE-striking set is more prominently developed on the regional scale but both sets show mutually abutting geometries on a local scale suggesting both sets were active concurrently (Flodin and Aydin, 2004). Faults of both sets dip steeply with mean dip angles of 80-90°. Following Myers (1999) and Flodin and Aydin (2004), the evolution of these faults includes the formation of joints, slip along joints, formation of splay fractures, and linkage of sheared joints.

These faults offset the Aztec/Willow Tank formation contact. Following the maps of Bohannon (1977) and Carpenter (1989) the youngest strata offset by faults of the Baseline fault system are the Miocene Horse Spring Formation and probably lower sections of the Upper Miocene Muddy Creek Formation (10-4 Ma, Bohannon et al., 1993). These faults are thus considered to be associated with Basin and Range tectonics (Flodin and Aydin, 2004).

DIAGENETIC ALTERATION

Methods

The distribution of diagenetic alteration of the Aztec Sandstone (Fig. 2) was mapped on color aerial photographs on a scale of 1:4,000 and extensively field checked. Rock color was determined using the Munsell Soil Color Charts (1994). For hues outside the range of the Soil Color Charts, the Rock Color Charts (Rock-Color Chart Committee, 1970) were used. Munsell and Rock Color names are given in combination with their numeric characterization of hue (shade), value (lightness), and chroma (saturation). The field designation of alteration units do not

follow these color names, however, because they do not distinguish among differences in hue that are significant in the context of this study.

Petrographic descriptions are based on 59 mostly polished sections of samples impregnated with blue epoxy under vacuum. Eleven representative samples of diagenetic alteration zones were collected for compositional analysis by powder X-ray diffraction (XRD) ICP-AES, and X-ray fluorescence (XRF). XRD samples were disaggregated in an agate mortar and the <2 μm size fraction separated following standard centrifuge techniques (Poppe et al., 2001). Oriented sample mounts of glycolated and unglycolated samples were scanned over 4-65° 2 θ at 1°/minute on a Rigaku powder diffractometer. Samples for elemental analysis were prepared by Li-tetraborate fusion and analyzed by ICP-AES at Actlabs-Skyline, Tucson, Arizona. Two samples were analyzed by X-ray fluorescence at Washington State University, Pullman, Washington, following the methods of Johnson et al. (1999). Ferrous iron was analyzed by Actlabs-Skyline, Tucson, Arizona, by titration with dichromate after HCl-HF acid digestion.

Compositional changes

The Aztec Sandstone is a fine to medium-grained subarkose (Marzolf, 1983) with up to 8% feldspar (Flodin et al., 2003) and a smaller amount of lithic components. The sandstone is generally friable with a porosity of 15-25% and permeability of 100-2500 md (Flodin et al. 2003). Grains are subrounded to rounded, characteristic of the eolian depositional environment. Throughout the section grains are weakly indented as a result of pressure solution and pore space is partially filled by clay cement (Fig. 3a). The predominant feldspar is orthoclase, observed in thin section in various stages of replacement by kaolin minerals. With the exception of one sample of high stratigraphic position (sample 04/04/01-3) that contained dickite, the dominant kaolin mineral was determined by X-ray diffraction to be kaolinite following criteria given by Lanson et al. (2002) (Table 1). Other clay minerals are mixed-layer illite/smectite. Kaolinite forms pore-filling clay and partially replaces K-feldspar. Kaolinite concretions are locally abundant. A notable occurrence is within an approximately 2 m thick bed of kaolinite-cemented sandstone (Fig. 2) that may represent a paleo-soil horizon. Kaolinite concretions are also found localized along faults indicative of syn- to post-faulting kaolinite remobilization. Mixed layer illite/smectite is 90% illite with a Reichweite of 3. In the stratigraphically lowest sample (99-20), illite replaces mixed layer illite/smectite.

Minor amounts of quartz overgrowth cement were observed in stratigraphically lower parts of the Aztec Sandstone. Quartz cement was also found locally within the damage zone and to both sides of the Bighorn fault (Fig. 2), cementing allochthonous Aztec Sandstone of the Willow Tank thrust sheet as well as fault rock that is part of the autochthonous Aztec Sandstone. Carbonate cement that is not attributed to modern caliche is found locally as pore-filling cement along joints and as concretions, both occurrences restricted to the lower part of the Aztec Sandstone.

The characteristic hues of red, orange, purple, yellow, and white of the Aztec Sandstone result from varying amounts and forms of iron oxide and hydroxide cement, the dominant pigments being hematite and goethite. The uniform red color (Munsell 10R 6/8 light red) of the lower red and upper red alteration units of the Aztec Sandstone results from thin grain coats of hematite. In thin section, hematite forms a mottled brownish coloration of grain surfaces (Fig. 3a). In samples of lower red sandstone containing quartz overgrowth cement, the hematite coat predates the quartz overgrowth indicative of an early diagenetic or syndepositional origin of the hematite coat.

Compared to grain coats in red sandstone, grain coats in yellow sandstone (Munsell 10YR 7/6 yellow to 10YR 8/2 very pale brown) are more patchy and partly recrystallized to ≤ 1 μm sized crystals (Fig. 3b). Based on X-ray diffractograms, the dominant Fe-oxide is goethite

(Table 1). This is consistent with goethite being the predominant pigment in yellow soils (Schwertmann, 1993). In orange-colored sandstone (Munsell 2.5 YR 5/8 red), hematite forms 5-10 μm sized globules that are attached to grain surfaces (Fig. 3c). The equally spaced distribution of hematite globules along grain surfaces is suggestive of globule formation by local dissolution of earlier grain coats and reprecipitation of hematite with accompanying crystal coarsening. Purple coloration (Rock Color Chart 5RP 6/2 pale red purple to 5RP4/2 grayish red purple and Munsell 10R 6/3 pale red) is caused by 1-3 μm sized grains of Fe oxide (Fig. 3d), identified by XRD to be dominantly goethite (Table 1). Some samples of purple and yellow sandstone also contain smaller amounts of the sulfates alunite $\text{KAl}_3(\text{SO}_4)_2(\text{OH})_6$ and jarosite $\text{KFe}_3(\text{SO}_4)_2(\text{OH})_6$. Jarosite provides a mottled brownish color to the otherwise uniform yellow sandstone. White sandstone (Munsell 10YR 8/1 to 7.5YR 8/1 white) is devoid of grain coats (Fig. 3e) but contains sparse flakes of coarse-crystalline hematite.

Joints and faults are frequently associated with haloes of dark red (Munsell 10R4/3 to 10R 4/4 weak red) pore-filling hematite. This type of hematite resembles hematite globules found in orange sandstone but occurs at higher density, completely occluding intergranular pores (Fig. 3f).

Elemental analyses of Aztec Sandstone (Table DR1) indicate that concentrations in Fe_2O_3 are <1%, including samples of lower and upper red sandstone. The only exception is one sample shown in Figure 3f containing pore-filling hematite with ~3% Fe_2O_3 . The elemental analyses generally lack systematic trends in Fe_2O_3 for samples of different hue. The differences in hue apparently reflect differences in mineral composition and grain size of Fe minerals rather than Fe concentration, in agreement with findings in soil science (Torrent and Schwertmann, 1987; Schwertmann, 1993).

Characterization of diagenetic alteration units

Myers (1999) and Flodin et al. (2003) subdivided the Aztec Formation at Valley of Fire State Park into three informal members, referred to as “lower red”, “middle beige” or “middle yellow”, and “upper orange” member. Although the boundaries of these rock units are subparallel to bedding on a regional scale we will show that they are diagenetic and not primary depositional in origin and thus not members in a stratigraphic sense. Instead, we subdivide the Aztec Sandstone into diagenetic alteration units to describe mappable sections of the formation of similar alteration color and color distribution.

The lower red alteration unit

In modification of the previous nomenclature we use the term lower red unit to designate the stratigraphically lower 800-900 m thick section of the formation that is stained uniformly red (Fig. 1). The red hue of the lower red unit is uniform without regard to grain size variations among cross-stratified layers. The only variation in color is associated with darker red bands resembling Liesegang bands. These bands are found locally within and adjacent to faults and are oblique to bedding and thus identified as a secondary alteration of the uniform red stain.

The boundary between the lower red to yellow and purple sandstone of the overlying middle alteration units is a relatively sharp transition in coloration (Fig. 4a) that occurs over 1-5 cm. Within this transition, the boundary appears frayed due to preferred reddening of finer-grained sandstone layers and the absence of red stain within coarser layers (Fig. 4b). Along the boundary the red sandstone is frequently somewhat darker (arrow in Fig. 4b) due to a larger grain size of hematite. Rather than being planar the upper boundary of the lower red unit has a lobate-cusped geometry, with lobes of purple or yellow sandstone penetrating the lower red sandstone (Fig. 4c). The boundary is parallel to bedding over distances of 10-100 m but frequently climbs, and occasionally drops, across bedding over distances of 10-50 m. In the Rainbow Vista area

(lower right section of Fig. 2), the average orientation of the boundary dips to the northeast by up to 49° compared to bedding at 22°.

The upper red alteration unit

The designation upper red unit is used to describe a 30-50 m thick section within the stratigraphically upper part of the Aztec Sandstone that resembles the lower red unit in its uniform red alteration color. Similar to the upper boundary of the lower red unit, the lower boundary of the upper red unit is parallel to bedding over distances of 10-30 m, then cuts upsection over similar distances at an angle of up to 20° relative to bedding. On average, this boundary dips 40° to the northeast compared to a bedding dip of 20-30° to the northeast.

The banded red and white unit

The upper red unit is overlain by a 30-60 m thick unit, referred to as banded red and white unit (Fig. 2), that is composed of red layers alternating with white layers (Fig. 4d). The boundary between the banded red and white unit with the underlying upper red unit frequently follows bedding but locally cuts obliquely across bedding. At those locations the white bands fade with an orange intermediate color into the uniform red stain. Approaching the Willow Tank thrust the red and white banding becomes irregular, with white patches and streaks cutting across bedding (Fig. 4e). The top 10-20 m of the banded red and white unit south of the Willow Tank thrust is bleached white to pink (Munsell 10R 8/3 to 2.5R 8/3 pink) (Fig. 2). In addition, the allochthonous Aztec Sandstone along the base of Willow Tank thrust sheet is bleached white (Fig. 4e, arrows).

The middle alteration units

Units of various colors between the lower and upper red units are referred to collectively as middle units. The middle alteration units include bands of white, yellow, purple, orange, and smaller amounts of red sandstone. Alteration bands too thin to be mapped as separate units were categorized as banded orange and white, banded purple and white, and banded purple and yellow (Fig. 2). The dominant portion of the banded units consists of banded orange and white sandstone. Similar to the banded red and white unit at the top of the Aztec Sandstone, the banding is manifest as an orange stain in the finer-grained sedimentary layers and the absence of pigment in the coarser-grained layers. This banding results in an alternating sequence of about 10-20 cm thick orange and white layers that follow depositional bedding. In addition, locally abundant deformation bands affected the distribution of pigment, acting as boundaries that separate compartments with internal color gradients from orange to white (Fig. 4f). The distribution of pigment in banded orange and white sandstone is thus controlled by both depositional layering and deformation bands.

Banded purple and white alteration resembles the banded orange and white alteration in the pattern of alteration except that orange pigment is replaced by purple. The boundary between banded orange and white and the banded purple and white alteration is gradational. Purple and white banding is observed in the vicinity of and in contact with the yellow and purple alteration units discussed next (Fig. 4g).

Purple, yellow, and banded purple and yellow alteration units are frequently observed to cut obliquely across banded orange and white and banded purple and white alteration with a sharp boundary. Purple bands in yellow sandstone frequently do not follow bedding. These bands are rather irregular with diffuse boundaries resembling schlieren or marbling in metamorphic or metasomatic rocks. Remnants or ghosts of stratigraphically controlled orange and white or purple and white banding may be locally recognizable in yellow and purple alteration units. These remnants as well as the crosscutting relations of the alteration unit boundaries indicate that banded orange and white alteration predates the yellow and purple alteration. Based on the spatial association of banded purple and white alteration along the boundary to the yellow and purple

alteration unit, we infer that the purple and white alteration is a secondary alteration of the orange and white alteration.

Bands of uniform white and orange alteration colors that are up to 20 m thick and thus mapped as separate units (Fig. 2) were found along and parallel with the base of the upper red alteration unit. In the northern part of the map area (Fig. 2), a 10-20 m thick white band lies below the upper red unit, followed by an equally thick orange band, and a second white band. The boundary between white and the upper red unit is locally sharp, changing from white to red within 1 cm (Fig. 4h). At other places, this boundary appears washed out and gradational over 1-2 m. The orange band below the upper red unit is roughly parallel to the lower boundary of the upper red unit. Whereas the upper boundary of the orange band is rather diffuse its lower boundary is typically sharp and accentuated by a 1-3 cm thick band of purple sandstone (Fig. 5a). This lower boundary forms lobes that protrude into the underlying white or yellow sandstone for 5-10 m (Fig. 5a). These lobes frequently follow joints (Fig. 5a) and where joints are reactivated in shear the boundaries of these lobes are offset (Fig. 5b).

Distribution of alteration units

The distribution of alteration units within the mapped area as seen in cross section is roughly symmetric (Fig. 6), with yellow and banded orange and white units in the center, overlain and underlain by purple and yellow and the red sandstone of the upper and lower red units. The symmetry is broken by the occurrence of white and orange bands along the boundary to the upper red unit, and by the banded red and white sandstone above the upper red unit.

Purple and yellow alteration thus occurs in three horizons within the middle alteration units, (1) in contact with the lower red alteration unit, (2) in the center of the middle alteration units, and (3) at the top of the middle alteration units. The central occurrence of yellow and purple sandstone forms a lobe that occupies most of the middle alteration units to the southeast and tapers off to the northwest. The top boundary of this lobe is less inclined than the other alteration bands allowing the overlying banded orange and white unit to increase in thickness toward the northwest (Fig. 6). To the northwest of the Bighorn fault the yellow and purple lobe climbs stratigraphically (Figs. 2 and 6).

CROSS-CUTTING RELATIONS AMONG ALTERATION UNITS AND DEFORMATION STRUCTURES

The spatial distribution of alteration units is affected by faults, joints, and deformation bands due to (a) structural offset of diagenetic boundaries and (b) localized alteration along these structural features. Structural offset of diagenetic boundaries is equal to the structural offset of stratigraphic markers if the diagenetic boundary predates fault slip, or less than the offset of stratigraphic markers if the diagenetic boundary formed while the fault was active. Localized alteration along faults or deformation bands can result in an apparent offset of diagenetic boundaries that can exceed the structural offset of stratigraphic markers along these structures. Localized alteration indicates that deformation preceded alteration. Both types of cross-cutting relations provide constraints on the relative timing of diagenetic alteration and flow processes that caused alteration. In addition, localized alteration provides evidence for the effects of structural heterogeneities on fluid flow through this sandstone unit.

Examples of structurally offset diagenetic boundaries are seen along the upper boundary of the lower red unit and the lower boundary of the upper red unit. Both boundaries are structurally offset by the two sets of strike-slip faults in the area, the NNE-striking left-lateral set and the NW-striking right-lateral set (Figs. 1, 2, and 5c). The structural offset of these alteration boundaries agrees with the offset of stratigraphic markers including dune boundaries and the basal conglomerate of the Willow Tank Formation (Flodin and Aydin, 2004). Thus, strike-slip faulting postdates these alteration boundaries.

Examples of apparent offsets due to localized alteration were observed along deformation bands that appear to offset the top boundary of the lower red alteration unit (Fig. 5d). However, these deformation bands lack any observable shear offset and are thus recognized as compaction bands. Taylor and Pollard (2000) explained the apparent offset of alteration boundaries across compaction bands by the relative retardation of a moving reaction front on one side of these bands relative to the other side. This interpretation implies that the alteration causing the red to yellow boundary is affected by the presence of the compaction band. Thus, the alteration boundary postdates the formation of the compaction bands.

The asymmetric alteration around deformation bands in the banded orange and white unit (Fig. 4f) described above is interpreted in a similar way. No slip is discernible across these bands (Hill, 1989) that would create a structural juxtaposition of orange next to white sandstone. Rather, diagenetic alteration of the sandstone appears localized adjacent to these bands.

Shear bands are observed to influence the bleaching within the banded red and white unit south of the Willow Tank thrust (Fig. 5e). These shear bands offset bedding planes by as much as 10 cm. Because bleaching is confined to certain layers of the cross-bedded sandstone, the red and white layers appear to be offset by the shear band. Bleaching is localized along these shear bands (arrows in Fig. 5e), however, indicating that alteration at least in part postdates the formation of these bands.

Joints can be associated with either localized precipitation of Fe oxides or localized bleaching (Fig. 5b and 5f). Figure 5b depicts hematite haloes around joints that have been subsequently sheared, thus offsetting the boundaries of the alteration halo by 2 cm. These haloes are along the lower boundary of the orange band that underlies the upper red unit. The formation of these joints thus predates this alteration boundary but shear along these joints postdates the alteration boundary.

The interaction of faults with the purple, orange, and yellow alteration zones is more complex. Rather than being physically offset, these alteration bands frequently turn to become parallel with these faults. The best example of this interaction is the apparent offset of the orange, white, yellow, and purple bands along the Bighorn fault immediately below the upper red unit (Fig. 2). Approaching the fault from the southeast, part of the orange band turns parallel with the fault and follows the fault for about 15 m (Fig. 7a, c). Similarly, the yellow and purple bands turn and follow the fault trace before crossing the fault (Fig. 2). This change in attitude of the alteration bands is not due to drag of bedding. Bedding does not noticeably change attitude adjacent to the fault. Rather, it appears that the purple and yellow bands approximately maintain a fixed distance relative to the upper red unit which is structurally offset along the Bighorn fault by 600 m of apparent left-lateral slip (Flodin and Aydin, 2004). The position of these bands is therefore affected by the presence of this fault and the diagenetic and fluid flow processes that resulted in these bands postdate most if not all of the structural offset of the upper red unit. This also suggests that the orange, purple, and yellow bands are secondary diagenetic modifications of the upper red boundary. Final stages of fault slip appear to have outlasted the formation of the orange band as indicated by the left-lateral offset of the lower boundary of the orange band along sheared joints (Fig. 5b). These joints appear to be part of the damage zone of the Bighorn fault or of an immediately adjacent subsidiary fault.

Purple and yellow sandstone of the central lobe within the middle alteration units appear to be deflected upward along the southeast side of the Bighorn fault and subsidiary faults (Fig. 6). Again, this deflection indicates that the faults were present at the time of the alteration.

Cross-cutting relations similar to those observed along the Bighorn fault are seen along the Lonewolf and Classic faults to the east (Figs. 2 and 6). In both cases, the upper red unit, including the banded red and white unit, are structurally offset by an amount consistent with the

offset of the overlying Willow Tank Formation. The apparent offset of the purple and yellow bands underneath the upper red unit can be explained by their tendency to follow the upper red unit without or with little structural offset. The shallowly inclined upper surface of the central yellow lobe has small structural offsets on the order of 1-10 m along these faults, about one order of magnitude less than their total apparent slip, indicating that fault slip outlasted the formation of alteration bands. The upper boundary of the lower red unit is, similar to the lower boundary of the upper red unit, structurally offset along these strike-slip faults. Along the Mouse's Tank fault, the lower red unit is structurally offset by 240 m of apparent left-lateral slip (Fig. 5c).

DISCUSSION

Interpretation of alteration units

Syn depositional reddening and first bleaching and remobilization stage

Following the petrographic studies of red beds in modern and ancient depositional settings by Walker et. al. (1978, 1981) we interpret the hematite grain coats resulting in the uniform red alteration of the lower and upper red units as an early syn depositional diagenetic alteration under near-surface conditions immediately following deposition. This syn depositional diagenetic origin may have included multiple cycles of deposition, alteration, and redeposition (Wilson, 1992). A syn depositional origin of the red stain is consistent with the abundant occurrence of clasts of red Aztec Sandstone in the basal conglomerate of the Willow Tank Formation (Longwell, 1949). A syn depositional origin of the red stain also is consistent with the uniform alteration color irrespective of grain size and porosity variations in cross beds or deformation bands within the red alteration units. Variations in permeability corresponding to variations in porosity would likely result in color variations if hematite precipitation were secondary within an initially white sandstone that had been reddened by advective transport of ferrous iron and subsequent oxidation. Instead, the uniform distribution of hematite is consistent with the in-situ breakdown of iron-containing silicates in an oxidizing environment and local precipitation of iron oxide coatings on the surfaces of chemically more resistant quartz grains, without the involvement of any significant post-depositional advective transport.

This alteration likely affected the entire formation resulting in a continuous sequence of red stained sandstone (Fig. 8a). We consider red kaolinite concretions within the middle alteration units (Fig. 5h) as vestiges of this initial red hematite stain, assuming that the tight kaolinite cementation of these concretions prevented the dissolution of hematite from within the concretions whereas the surrounding permeable sandstone was preferentially bleached. Hematite grain coats also provided the precursor iron minerals to re-precipitated hematite and goethite cements in the middle alteration units.

The secondary origin of the middle alteration units relative to the homogeneous red of the lower and upper red units is deduced from the nature of the lobate-cusped shape of the boundary between the red and middle alteration units. Lobes along the lower red boundary (Fig. 4c) point into the red sandstone whereas cusps point into the overlying yellow sandstone. This suggests that the reaction boundary moved into the red sandstone, presumably due to fingering of a reducing alteration front or "side".

The occurrence of slightly darker sandstone along this diagenetic alteration boundary (Fig. 4b) is consistent with coarsening of hematite immediately ahead of the reducing front. Coarsening, also referred to as Ostwald ripening, results from the tendency of forming energetically more favorable large crystals during repeated dissolution and reprecipitation (Lasaga, 1998). The dependence of hematite solubility on crystal size, with small crystals being more soluble than larger crystals, was recently reviewed by Cornell and Schwertman (2003). Thus, coarsening would result from local supersaturation of the fluid for hematite of large crystal size even though the fluid is undersaturated relative to the bulk of smaller, and possibly

amorphous (Walker et al., 1978), hematite forming the grain coats. Immediately ahead of the advancing reduction front some initially larger hematite crystals grew at the expense of smaller crystals that got dissolved (Fig. 9). Due to the effect of hematite crystal size on alteration color (Torrent and Schwertman, 1987), this zone became darker red. As the reduction front advanced further, the fluid eventually became undersaturated even for larger hematite crystals and all hematite went into solution. When the reduction front stopped propagating a darker rim of hematite remained.

A similar process can be invoked for the bands of white and orange following the lower boundary of the upper red unit. The difference to the above scenario lies in the coarsening of few remaining larger hematite crystals behind, rather than ahead of, the reduction front. Coarsening is consistent with the larger size of hematite crystals in orange sandstone compared to red sandstone as observed in thin section. The first band of white sandstone separating uniform red and striped orange sandstone is thus interpreted as the result of a kinetic lag between dissolution and reprecipitation. With continued advancement of the reduction front undersaturation was reached even for those larger grains resulting in the secondary dissolution of the larger hematite grains and the formation of the second white band below and behind the orange band. We thus interpret the orange band below the upper red boundary to have initially formed during the first alteration stage as the byproduct of bleaching of the upper red unit. The orange band was partially remobilized during a later second stage of alteration, with its lower boundary migrating preferentially along joints (Fig. 5a).

The boundaries of the lower and upper red units to the middle alteration units clearly predate faulting but, as shown above, postdate compaction bands. The cross-cutting of the banded orange and white alteration with strike-slip faulting is not clear although faults do not affect the intensity of the banding which thus appears to predate strike-slip faulting. The alteration of the banded orange and white unit postdates deformation bands because these bands form the boundaries to the alteration compartments that are characteristic of this unit. No younger set of deformation bands is observed that does not interact with the banded orange and white alteration. The hematite resulting in the orange color of the banded orange and white unit is similar to the hematite in the orange unit and thus is considered a secondary alteration product.

We also consider the alteration reactions observed in the banded red and white unit to be part of the first stage of bleaching and remobilization (Fig. 8b). The banded red and white unit is mechanically offset by the strike-slip faults which also offset the Willow Tank thrust. Bleaching at the top of the upper red unit is spatially associated with the Willow Tank thrust. This bleaching also postdates shear bands. We attribute the bleaching within the banded red and white sandstone to the proximity to the overlying gray and organic-rich mudstones of the Cretaceous Willow Tank Formation, with the bleaching being enhanced below and in the vicinity of the Willow Tank thrust sheet.

Bleaching of the red sandstone by the dissolution of hematite grain coats requires that the fluid composition shifted toward more reducing and/or acidic conditions (Fig. 10). Such a shift likely resulted from the influx of basinal fluids that had been in contact with organic-rich sediment or hydrocarbons. We thus infer the first bleaching and remobilization stage to be associated with the flow of reducing and/or more acidic basinal fluids. High concentrations of organic acid, methane, or hydrogen sulfide that are common in such fluids would have provided favorable conditions for hematite dissolution (Chan et al., 2000).

Second bleaching and remobilization stage

The second bleaching and remobilization stage resulted in remobilization of iron oxides and iron hydroxides within and along the boundaries of the first alteration stage (Fig. 8c). The products of this alteration stage include the yellow and purple alteration colors as well as the local

remobilization of the orange layer below the upper red unit. All these alteration products overprint or cross-cut the alteration products attributed to the first bleaching and remobilization stage. Based on the cross-cutting relations with faults, this second alteration stage occurred during strike-slip faulting. The sub-horizontal upper boundary of the yellow lobe in the center of the middle alteration units also suggests that this alteration occurred after tilting of the Aztec Sandstone to the northeast.

This second stage of bleaching and remobilization is characterized by the common occurrence of goethite and minor alunite and jarosite. At temperatures below 100°C and unit water activity, coarse-grained goethite is considered the thermodynamically stable phase (Cornell and Schwertman, 2003). The precipitation of goethite rather than hematite is favored at low pH of about 4 and high pH of about 12 whereas a neutral pH of about 8 favors the formation of hematite (Schwertman, 1985). Under partially saturated conditions, hematite is favored relative to goethite with decreasing water activity or humidity (Torrent et al., 1982; Schwertman and Taylor, 1989). In soils, low temperatures, high Al and H₂O activity, and higher organic content favor goethite precipitation (Schwertman and Taylor, 1989). Small particle size favors the stability of hematite (Schwertman and Taylor, 1989). Perhaps most significant for the occurrence of goethite under subsurface conditions is the laboratory observation that hematite precipitation requires the precipitation of ferrihydrite as a precursor phase, a poorly ordered iron hydroxide of composition Fe_{1.55}O_{1.66}(OH)_{1.33} (Cornell and Schwertman, 2003), whereas goethite can precipitate directly from solution (Schwertman and Taylor, 1989). Goethite will thus be favored over hematite due to sluggish reaction kinetics even under conditions where equilibrium considerations would predict hematite stability. While the complexity of the hematite-goethite system makes it difficult to ascribe the replacement of hematite by goethite within the Aztec Sandstone to a specific environmental factor, it can be concluded that this replacement would be favored by a decrease in temperature, a decrease in pH, and a decrease in water saturation under undersaturated conditions.

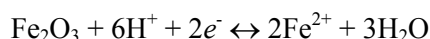
The sulfates alunite KAl₃(SO₄)₂(OH)₆ and jarosite KFe₃(SO₄)₂(OH)₆ frequently form as the result of pyrite oxidation in organic-rich shales that are in contact with acidic oxidized water (Langmuir, 1997). The Aztec Sandstone, deposited subaerially under oxygenated conditions, clearly did not contain primary or early diagenetic sulfide. Any sulfur that is now contained in alunite and jarosite must have been brought into the system by migrating fluids. Jarosite is stable under acidic and strongly oxidizing conditions (Fig. 10). In the sulfate system containing Al, K, and Fe, alunite is stable under somewhat lower p_e conditions compared to jarosite.

A possible scenario that combines reducing conditions resulting in bleaching with suitable conditions for sulfate precipitation involves the upward migration of reducing sulfide-rich basal fluids and mixing with oxidizing meteoric waters. As shown in the p_e-pH diagram (Fig. 10) the reaction of hematite with sulfide-rich low- to intermediate-p_e fluids would lead to the dissolution of hematite without necessarily precipitating pyrite provided pH conditions are sufficiently low and the system is not too strongly reducing. Under those conditions iron goes in solution as Fe²⁺. The abundance of hematite may have buffered the system sufficiently to prevent pyrite formation which is not observed as mineral phase or pseudomorph. We suggest that oxidizing conditions necessary for the precipitation of jarosite and alunite were met during subsequent mixing of the reduced sulfide-rich basal fluid with oxidizing meteoric water. The associated increase in p_e would have moved the system into the jarosite field, and, under high Al activities, alunite stability field, whereas an increase in both p_e and pH would have resulted in the precipitation of amorphous iron hydroxide that may then have been converted to goethite or hematite. Under kinetically favorable conditions, goethite would have precipitated directly from solution without the amorphous iron hydroxide precursor, thus competing with the precipitation of jarosite. The p_e-pH conditions may have varied locally resulting in varying amounts of sulfides being precipitated.

Based on the cross-cutting relations of sulfate-containing yellow and purple alteration bands with faulting we thus ascribe the second bleaching and remobilization stage to meteoric water entering the aquifer and mixing with basinal fluid.

Inferred paleo-flow direction

Criteria that constrain the direction of paleo-fluid flow in the Aztec Sandstone include the asymmetry of alteration adjacent to deformation bands in the banded orange and white unit (Figs. 4f, 11a, b). The orientation of preferred reddening or bleaching adjacent to deformation bands in the banded orange and white unit appears locally uniform. This consistency in the orientation of asymmetric alteration around deformation bands suggests that this asymmetry reflects the local orientation of reactive fluid flow. We hypothesize that the asymmetric reddening and bleaching, and in particular the “ponding” of red alteration at intersecting deformation bands (Figs. 11a, b), resulted from solute sieving across deformation bands that acted as geologic membranes for ions in solution. Such membrane behavior, suggested by Whitworth et al. (1999) for faults in sandstone, would increase the activity of dissolved ions on the upstream side relative to the downstream side. For the reaction



the activity for Fe^{2+} ions is expected to be higher on the upstream side of deformation bands, resulting in preferred hematite growth, or a lesser extent of hematite dissolution, compared to the downstream side of deformation bands where hematite precipitation would be impeded or dissolution enhanced.

To test if the direction of preferred reddening and thus the inferred direction of reactive fluid flow is uniform over the mapped area, we measured the orientation of deformation bands and the associated orientation of preferred reddening or bleaching at two locations within the banded orange and white unit. Data were collected over an outcrop area of approximately 500 m² at location A and 200 m² at location B (Fig. 2). Data collection was aimed at obtaining a uniform spatial distribution of deformation band orientations by including less common bands with orientations that deviate from the three dominant sets described by Hill (1989). Nonetheless, the data sets fall into two distinct sets that strike NNW-SSE and ENE-WSW, respectively, when plotted as great circles on an equal angle stereographic projection (Fig. 11c, d).

For each great circle in Figures 11c and d, the side corresponding to the bleached face of the deformation band is marked blue and the side corresponding to the red face is marked red. Assuming that fluid flow and thus the diagenetic alteration around bands is not influenced by neighboring bands we assume that deformation band compartments that contain the approaching flow vector should be characterized by consistently inward-facing red faces (Fig. 11b). If the compartment is oriented in an oblique direction relative to the flow vector, the faces defining the compartment would consist of both red and bleached faces.

At both locations that were investigated multiple compartments consistently had reddened or bleached faces (Fig. 11c and d). These are marked in Figure 11 by light red or light blue shading, respectively. A unique flow orientation is obtained at both locations, however, by additionally requiring that these compartments are enclosed in a larger compartment with same consistent reddened or bleached faces. For each of the two locations we find only one compartment that meets this criterion, marked in Figure 11c and d as containing the inferred flow direction. At both locations, the flow direction obtained using this graphical technique trends NE-SW and plunges to the NE. Whereas at location A this direction corresponds to a downward flow of reducing fluid, the opposite flow direction is inferred for location B. Apparently, this technique yields consistent results on an outcrop scale but inferred flow directions are variable at the kilometer scale.

Flow direction indicators for other alteration units include oxidation trails around oxide concretions and lobate alteration boundaries. Tails around iron oxide concretions (Fig. 5g) indicate downward and SE-directed migration of a purple alteration front south of Pt. 685 (Fig. 1). The lower boundary of the orange layer that underlies the upper red unit forms lobes that had migrated down section (Fig. 5a). In both cases, the direction of the tails or lobes is interpreted to reflect the direction of advective mass transfer and thus the fluid flow direction.

Fluid flow, alteration, and correlation with regional tectonics

The correlation of deformation bands with Sevier thrusting suggested by Hill (1989) and Flodin and Aydin (2004) provides a lower time constraint for the onset of basinal fluid expulsion during the first stage of bleaching and remobilization (Fig. 8b). In addition, the spatial correlation of bleaching in the upper red unit with the Willow Tank thrust requires that the thrust sheet be in place by the time of alteration. An upper time constraint for the first stage of bleaching and remobilization is provided by strike-slip faulting and tilting of the sequence during Miocene times. Basinal fluids were likely to be expelled due to the increase in burial associated with the emplacement of the thrust sheets and concurrent to subsequent deposition of detrital units in the foreland. We estimate that the maximum burial depth of the Aztec formation top corresponds closely to the thickness of the post-Jurassic units to the east, amounting to about 1600 m. The occurrence of quartz overgrowth cement and diagenetic illite in the lowermost part of the Aztec Sandstone, typically requiring burial temperatures in excess of about 80°C (Worden and Morad, 2000, 2003), appears consistent with this estimate. The geothermal gradient could have been elevated along the thrust front due to fluid flow, consistent with the occurrence of quartz cement and dickite in close proximity and below the Willow Tank thrust sheet. With the exception of the Willow Tank thrust, the post-Jurassic sequence on top of the Aztec Sandstone clearly indicates that the thrust sheets did not extend to the eastern part of the study area. The exposed leading edge of the Willow Tank thrust sheet and a right-lateral tear fault along its southern edge (Longwell, 1949) makes it likely that most of the area shown in Figure 2 was not covered by the Willow Tank thrust. Continuous Cretaceous sedimentation on top of the Aztec Sandstone south of the Willow Tank thrust excludes that the Aztec Sandstone shown in Figure 2 was covered by the next higher thrust sheet, the Muddy Mountain thrust sheet. Connecting the closest erosional remnants of the Muddy Mountain thrust sheet, as defined by Bohannon (1983), to the west and southeast of the study area places the front of the Muddy Mountain thrust approximately along the western boundary of the detailed map area (Fig. 2). With the study area located ahead of the thrust sheets, expulsion of basinal fluids could thus have started with the advancement of the orogenic front and reached a maximum with maximum burial prior to regional tilting and deposition of the Miocene Muddy Creek Formation. Following Bohannon (1983) the upward coarsening of the Cretaceous sequence recorded the eastward progression of the Sevier thrust sheets, with the coarsest deposits of the Upper Cretaceous Overton Conglomerate Member of the Baseline Sandstone corresponding to the final stages of thrusting.

The two paleo-flow direction analyses for this first fluid flow stage as determined in the banded orange and white unit indicate NE-SW-trending flow vectors but opposite polarity. Restoring the Aztec Sandstone into its untilted pre-Miocene position results in sub-horizontal formation contacts and sub-horizontal boundaries of the lower red to middle alteration units and of the middle alteration units to upper red alteration unit. This restoration rotates the flow vectors into subhorizontal positions that are approximately normal to the southeasterly thrusting direction of the Willow Tank thrust and approximately parallel to the inferred trend of the orogenic front. The opposite polarity of the flow vectors suggest that the direction of flow was locally variable. On a regional, i.e. basin-wide, scale fluid flow would be expected to be directed away from the axis of greatest rate of increase in overburden thickness and topographic elevation and thus from the orogenic front toward the foreland (Fig. 8b) (Oliver, 1986; Sverjensky and Garven, 1992)

The syn- to post-strike-slip faulting age of the second bleaching and remobilization stage and the sub-horizontal orientation of the top boundary of the middle yellow unit place the influx of meteoric fluids in Miocene to post-Miocene times (Fig. 8c). A younger cut-off is provided by the formation of modern topography that truncates the yellow and purple alteration units of the second alteration stage. The influx of meteoric fluids is likely the result of an increase in topographic head with the exhumation of the Muddy Mountains and the incision of the Colorado River, the latter inferred to initiate at about 5 Ma (Lucchitta, 1987). A topographic drive for meteoric water flow is consistent with flow direction indicators described above that suggest that the direction of fluid movement was down-dip and to the southeast.

The distribution of yellow and purple units likely reflects the dependence of hematite dissolution and goethite precipitation on the hematite distribution inherited from the first alteration stage as well as the focusing of meteoric water and basinal fluid within the sandstone formation. The crystallinity and abundance of hematite formed during the first bleaching and remobilization stage would control the saturation state and local Fe activity in solution and thus the remobilization of iron during the second bleaching and remobilization stage. Focusing of fluid flow would affect the mixing ratio of meteoric water and basinal fluid and thus the local fluid composition, including p_e and pH, the water/rock ratio, and the velocity and residence time of the migrating fluid within the formation.

The lobate shape of the central yellow unit tapering off to the northwest could reflect the interfingering of the two fluids present during the second bleaching and remobilization stage, i.e. reducing basinal fluid moving up-dip, and meteoric water moving down-dip. The position of this lobe probably follows the most permeable part of the middle alteration units. The shape of the lobe could mimic the plume of denser basinal fluid interfingering with lighter meteoric water. Thus, whereas the overall configuration of the alteration units is, to first approximation, controlled by the tilted formation boundaries, we interpret the subhorizontal upper boundary of the central yellow lobe to follow a hydraulic equipotential surface. This interpretation of the central lobe as a plume of basinal fluid requires that the migration of basinal fluid continued during the second bleaching and remobilization stage.

We interpret the lower and upper yellow and purple bands within the middle alteration units to be secondary modifications of the boundaries separating the lower and upper red units from the middle alteration units. The upper yellow and purple bands locally replace the white and orange bands that are interpreted to have formed during the first bleaching and remobilization stage. Compared to hematite in the homogeneous lower and upper red units, hematite in the orange bands may have been more conducive to secondary dissolution and reprecipitation during the second bleaching and remobilization stage, resulting in remobilization of the boundaries of the orange unit and, at a more advanced stage, alteration to purple and yellow goethite-containing sandstone.

Effect of structural heterogeneities on fluid flow

While the regional distribution of the lower red, middle, and upper red alteration units is controlled by stratigraphic contacts, structural features have a strong effect on the focusing of flow and alteration on scales ranging from <1 km to the outcrop and hand sample scale. The effect of map scale faults on fluid flow and alteration is best illustrated along the Bighorn fault and associated faults, deflecting the purple and yellow alteration units (Fig. 6). We suggest that this deflection results from impeded flow and thus limited transport of solutes across these faults. Fault hydraulic properties were determined by Flodin et al. (2004) who measured a one to three orders of magnitude reduction in fault permeability for flow across these faults compared to the host sandstone. Although faults apparently acted as aquitards for cross-fault flow, the locally enhanced precipitation of iron oxides and hydroxides along these faults within otherwise bleached

sandstone that is juxtaposed against red sandstone suggests that iron in solution may have “bled” through these faults. Along the Bighorn fault, this localized alteration is observed in the central yellow and purple alteration units as well as in the upper orange unit (Fig. 7a, c), in both cases on the SE side of the Bighorn fault. We consider this preferred bleeding of iron onto the SE side of the fault as additional evidence for the SE directed flow of meteoric fluid during the second alteration stage.

The partial sealing character of these faults has been explained by Flodin et al. (2004) by the significant grain size reduction associated with fault slip. Diagenetic sealing effects were considered to be minimal although localized kaolinite precipitation along these faults is clearly observed (Fig. 7b). Permeability parallel to these faults within the fault damage zone was found by Jourde et al. (2002) to be higher by up to one order of magnitude. Enhanced flow along these faults would have contributed to the deflection and parallel alignment of alteration zones along these faults.

Myers (1999) and Flodin and Aydin (2004) described in detail the process of fault formation by the opening of joints, subsequent shearing of these joints and formation of splay fractures, and linkage of sheared joints. Slip along these joint-based faults resulted in cataclasis and thus in a reduction in cross-fault permeability. The reactivation of single joints in shear, on the other hand, tends to increase the permeability of these joints due to the dilatant increase in joint aperture and the linkage with other joints, resulting in increased flow pathway connectivity. Sheared joints are thus frequently found to be associated with haloes of Fe oxides (Fig. 5b) whereas adjacent unsheared and isolated joints are barren (Taylor et al., 1999). The significance of these processes for the permeability structure of joint networks in the Aztec Sandstone was assessed by Taylor et al. (1999) using numerical simulations.

The effect of deformation bands on fluid flow is well illustrated by their interaction with alteration in the banded orange and white sandstone, indicating they acted as barriers to fluid flow. This is consistent with measurements of deformation band permeability by Antonellini et al. (1994) and Sigda et al. (1999) who found a permeability reduction for flow across deformation bands of up to three orders of magnitude compared to the undeformed sandstone.

The marked increase in deformation band abundance correlating approximately with the upper boundary of the lower red unit was noted by Flodin et al. (2003) and attributed to an increase in porosity from 12-20% in the lower red sandstone to 20-24% in the middle alteration units. We suggest that a higher porosity in the middle alteration units not only favored the formation of deformation bands but also resulted in focused fluid flow and enhanced alteration in the upper section of the Aztec Sandstone. Flodin et al. (2003) measured an increase in permeability in the middle alteration units by up to one order of magnitude compared to the lower red unit. This difference could have been lower or higher when diagenetic alteration of the middle units started due to later changes in pore filling cement. Nonetheless, their measurements are consistent with our conclusion that the middle alteration units acted as preferred pathways for fluid migration. However, this conclusion does not exclude fluid flow across the lower red unit. Alteration features are, in fact, observed in the lower red unit as described above. However, flow velocity and thus fluid volume may have been restricted sufficiently across the lower red unit to prevent significant hematite dissolution and bleaching of the formation.

CONCLUSIONS

Red, orange, yellow, and purple alteration bands in the Aztec Sandstone are associated with distinct forms of iron oxide and hydroxide. Red and orange colors result from hematite of different crystal size, yellow and purple colors from goethite. A uniform red stain resulting from thin grain coats of hematite is attributed to syndepositional dissolution of Fe-bearing detrital mineral phases and hematite precipitation. Based on mutual cross-cutting relations of orange,

yellow, purple, and white alteration bands and their interaction with faults, joints, and deformation bands we distinguish two stages of dissolution or bleaching, remobilization, and re-precipitation of iron oxides and hydroxides. The first bleaching and remobilization stage postdates deformation band formation but predates strike-slip faulting. This alteration stage is interpreted to be the result of the expulsion of reducing basinal fluids during and after emplacement of Sevier thrusts and the deposition of clastic foreland sediments. During this stage alteration resulted in extensive bleaching at the top of the Aztec Sandstone and partial re-precipitation of hematite in the banded orange and white unit. The second bleaching and remobilization stage resulted in the precipitation of predominantly goethite and minor amounts of the sulfates jarosite and alunite. This alteration stage occurred while the strike-slip faults were active and is attributed to the influx of meteoric water and its interaction with reducing, sulfide-rich basinal fluids.

Whereas the regional scale of fluid migration was controlled by formation contacts, thrust faults, and depth variations in porosity, local alteration patterns are strongly influenced by structural heterogeneities in addition to the sedimentary architecture. The interaction of fluid flow with deformation bands and bedding resulted in complex asymmetric alteration patterns in the banded orange and white unit during the first stage of bleaching and remobilization. Alteration haloes around sheared joints illustrate the significance of shearing and joint linkage for flow focusing along fracture networks. The local alignment of yellow and purple alteration bands along faults reflects the retardation of flow across these faults. These faults, formed by progressive stages of joint opening, joint shearing, and linkage, acted as aquitards for cross-fault flow due to extensive grain size reduction in the fault core and as fluid pathways for along-fault flow due to well developed damage zones.

The complex interaction of alteration bands with structural heterogeneities and thrusting illustrate the coupling among fluid flow, diagenesis, regional scale tectonism, and brittle deformation in subsurface fluid flow systems.

ACKNOWLEDGEMENTS

This study was financially supported by US Department of Energy grant DE-FG 03-94ER14462. We thank the rangers of the Valley of Fire State Park for logistic support and Eric Flodin, Kurt Sternlof, Jim Boles, and Rod Myers for discussions. Reviews by Martha Gerdes, Wanda Taylor, Peter Vrolijk, Peter Mozley, and Nancy Riggs are thankfully acknowledged.

REFERENCES CITED

- Antonellini, M. A., and A. Aydin, 1994, Effects of faulting on fluid flow in porous sandstones: petrophysical properties: AAPG Bulletin, v. 78, p. 355-377.
- Bethke, C. M., 2002, The Geochemist's Workbench. For Microsoft Windows. Release 4.0.2: Distributed by RockWare Earth Science Software, Golden, Colorado, 1 CD-ROM.
- Bohannon, R.G., 1977, Geologic map and sections of the Valley of Fire region, North Muddy Mountains, Clark County, Nevada: U. S. Geological Survey Miscellaneous Field Studies Map MF-849.
- Bohannon, R.G., 1983, Mesozoic and Cenozoic tectonic development of the Muddy, North Muddy, and northern Black Mountains, Clark County, Nevada: Geological Society of America Memoir, v. 157, p. 125-148.
- Bohannon, R.G., Grow, J.A., Miller, J.J., and Blank, R.H. Jr., 1993, Seismic Stratigraphy and tectonic development of Virgin River depression and associated basins, southeastern Nevada and northwestern Arizona: Geological Society of America Bulletin, v. 105, p. 501-520.
- Carpenter, D.G., 1989, Geology of the North Muddy Mountains, Clark County Nevada, and regional structural synthesis: fold-thrust and Basin-Range structure in southern Nevada,

- southwest Utah and northwest Arizona [M.S. Thesis]: Corvallis, Oregon State University, 145 p.
- Carpenter, D.G., and Carpenter, J.A., 1994, Fold-thrust Structure, Synorogenic Rocks, and Structural Analysis of the North Muddy and Muddy Mountains, Clark County, Nevada, *in* Dobbs, S.W., and Taylor, W.J., eds., Structural and Stratigraphic Investigations and Petroleum Potential of Nevada, with Special Emphasis South of the Railroad Valley Producing Trend: Nevada Petroleum Society 1994 Conference Volume II: Reno, Nevada, Nevada Petroleum Society, p. 65-94.
- Chan, M. A., Parry, W. T., and Bowman, J. R., 2000, Diagenetic Hematite and Manganese Oxides and Fault-Related Fluid Flow in Jurassic Sandstones, Southeastern Utah: AAPG Bulletin, v. 84, p. 1281-1310.
- Cornell, R. M., and Schwertmann, U., 2003, The Iron Oxides. Structure, Properties, Reactions, Occurrences and Uses, 2nd ed.: Weinheim, Wiley-VCH, 664 p.
- Doner, H. E., and Lynn, W. C., 1989, Carbonate, Halide, Sulfate, and Sulfide Minerals, *in* Dixon, J. B., and Weed, S. B., eds., Minerals in Soil Environments. 2nd edition: Madison, Wisconsin, Soil Science Society of America, p. 279-330.
- Flodin, E. A., and Aydin, A., 2004, Evolution of a strike-slip fault network, Valley of Fire State Park, southern Nevada: Geological Society of America Bulletin, v. 116, 42-59.
- Flodin, E. A., Prasad, M., and Aydin, A., 2003, Petrophysical constraints on deformation styles in Aztec Sandstone: Pure and Applied Geophysics, v. 160, 1589-1610.
- Flodin, E. A., Gerdes, M., Aydin, A., and Wiggins, W. D., 2004, Petrophysical properties and sealing capacity of fault rock from sheared-joint based faults, Aztec sandstone, Nevada, *in* Tsuji, Y., and Sorkhabi, R., eds., Fault Seals and Petroleum Traps, AAPG Memoir, in press.
- Hill, R.E., 1989, Analysis of deformation bands in the Aztec Sandstone, Valley of Fire State Park, Nevada [M.S. Thesis]: Las Vegas, University of Nevada, 68 p.
- Johnson, D. M., Hooper, P. R., and Conrey, R. M., 1999, XRF Analysis of Rocks and Minerals for Major and Trace Elements on a Single Low Dilution Li-tetraborate Fused Bead: Advances in X-ray Analysis, v. 41, p. 843-867.
- Jourde, H., Flodin, E.A., Aydin, A., Durlofsky, L.J., and Wen, X.-H., 2002, Computing permeability of fault zones in aeolian sandstone from outcrop measurements: AAPG Bulletin, v. 86, p. 1187-1200.
- Langmuir, D., 1997, Aqueous Environmental Geochemistry: Upper Saddle River, New Jersey, Prentice Hall, 600 p.
- Lanson, B., Beaufort, D., Berger, G., Bauer, A., Cassagnabere, A., and Meunier, A., 2002. Authigenic kaolin and illitic minerals during diagenesis of sandstones: a review: Clay Minerals, v. 37, p. 1-22.
- Lasaga, A., 1998, Kinetic Theory in the Earth Sciences: Princeton, Princeton University Press, 811 p.
- Longwell, C. R., 1949, Structure of the northern Muddy Mountain area, Nevada: Geological Society of America Bulletin, v. 60, p. 923-967.
- Lucchitta, I., 1987, The mouth of the Grand Canyon and edge of the Colorado Plateau in the Upper Lake Mead area, Arizona, *in* Beus, S. S., ed., Centennial Field Guide Volume 2: Rocky Mountain Section of the Geological Society of America, p. 365-370.
- Marzolf, J., 1983, Changing wind and hydraulic regimes during deposition of the Navajo and Aztec sandstones, Jurassic (?) southwestern United States, *in* M.E. Brookfield, and Ahlbrandt, T.S., eds., Eolian sediments and processes: Amsterdam, Elsevier, p. 635-660.
- Marzolf, J. E., 1990, Reconstruction of extensionally dismembered early Mesozoic sedimentary basins; Southwestern Colorado Plateau to the eastern Mojave Desert, *in* Wernicke, B. P., ed., Basin and Range extensional tectonics near the latitude of Las Vegas, Nevada: Geological Society of America Memoir, v. 176, p. 477-500.

- Mollema, P. N., and Antonellini, M. A., 1996, Compaction bands: a structural analog for anti-mode I cracks in aeolian sandstone: *Tectonophysics*, v. 267, p. 209-228.
- Moore, J. C., 1999, Fluid Seeps at Continental Margins-A Meeting Report: *Margins Newsletter*, v. 4, p. 12-14.
- Munsell Soil Color Charts, 1994, revised edition: New Windsor, New York, Munsell Color.
- Myers, R.D., 1999, Structure and hydraulics of brittle faults in sandstone [Ph.D. Thesis]: Stanford, Stanford University, 176 p.
- Oliver, J., 1986, Fluids expelled tectonically from orogenic belts: Their role in hydrocarbon migration and other geologic phenomena: *Geology*, v. 14, p. 99-102.
- Poppe, L. J., Paskevich, V. F., Hathaway, J. C., and Blackwood, D. S., 2001, A Laboratory Manual for X-Ray Powder Diffraction: U. S. Geological Survey Open-File Report 01-041, 1 CD-ROM.
- Rock-Color Chart Committee, 1970, Rock-Color Chart, Reprint: Boulder, Colorado, The Geological Society of America.
- Schwertman, U., 1985, Occurrence and formation of iron oxides in various pedoenvironments, *in* Stucki, J. W., Goodman, B. A., and Schwertman, U., eds., *Iron in Soils and Clay Minerals*: Dordrecht, Netherlands, Reidel Publishing, p. 267-308.
- Schwertman, U., 1993, Relations between Iron Oxides, Soil Color, and Soil Formation, *in* Bigham, J. M., and Ciolkosz, E. J., eds., *Soil Color: Soil Science Society of America Special Publication*, v. 31, p. 51-69.
- Schwertman, U., and Taylor, R. M., 1989, Iron Oxides, *in* Dixon, J. B., and Weed, S. B., eds., *Minerals in Soil Environments*, 2nd Edition: Madison, Wisconsin, Soil Science Society of America, p. 379-438.
- Sigda, J. M., Goodwin, L. B., Mozley, P. S., and Wilson, J. L., 1999, Permeability Alteration in Small-Displacement Faults in Poorly Lithified Sediments: Rio grande Rift, Central New Mexico, *in* Haneberg, W. C., Mozley, P. S., Moore, J. C., and Goodwin, L. B., eds., *Faults and Subsurface Fluid Flow in the Shallow Crust: Geophysical Monograph*, v. 113, Washington D. C., American Geophysical Union, p. 51-68.
- Sverjensky, D. A., and Garven, G., 1992, Tracing great fluid migrations: *Nature*, v. 356, p. 481-482.
- Taylor, W. L., and Pollard, D. D., 2000, Estimation of in situ permeability of deformation bands in porous sandstone, Valley of Fire, Nevada: *Water Resources Research*, v. 36, p. 2595-2606.
- Taylor, W. L., Pollard, D. D., and Aydin, A., 1999, Fluid flow in discrete joint sets: Field observations and numerical simulations: *Journal of Geophysical Research*, v. 104, p. 28983-29006.
- Torrent, J., Guzman, R., and Parra, M. A., 1982, Influence of relative humidity on the crystallization of Fe(III) oxides from ferrihydrite: *Clays and Clay Minerals*, v. 30, p. 337-340.
- Torrent, J., and Schwertmann, U., 1987, Influence of Hematite on the Color of Red Beds: *Journal of Sedimentary Petrology*, v. 57, p. 682-686.
- Trolard, F., and Tardy, Y., 1987, The stabilities of gibbsite, boehmite, aluminous goethites and aluminous hematites in bauxites, ferricretes and laterites as a function of water activity, temperature and particle size: *Geochimica et Cosmochimica Acta*, v. 51, p. 945-957.
- Walker, T. R., Larson, E. E., and Hobblitt, R. P., 1981, Nature and Origin of Hematite in the Moenkopi Formation (Triassic), Colorado Plateau: A Contribution to the Origin of Magnetism in Red Beds: *Journal of Geophysical Research*, v. 86, p. 317-333.
- Walker, T. R., Waugh, B., and Grone, A. Y., 1978, Diagenesis in first-cycle desert alluvium of Cenozoic age, southwestern United States and northwestern Mexico: *Geological Society of America Bulletin*, v. 89, p. 19-32.

- Whitworth, T. M., Haneberg, W. C., Mozley, P. S., and Goodwin, L. B., 1999, Solute-Sieving-Induced Calcite Precipitation on Pulverized Quartz Sand: Experimental Results and Implications for the Membrane Behavior of Fault Gouge, *in* Haneberg, W. C., Mozley, P. S., Moore, J. C., and Goodwin, L. B., eds., *Faults and Subsurface Fluid Flow in the Shallow Crust: Geophysical Monograph*, v. 113, Washington D. C., American Geophysical Union, p. 149-158.
- Wilson, M. D., 1992, Inherited Grain-Rimming Clays in Sandstones from Eolian and Shelf Environments: Their Origin and Control on Reservoir Properties, *in* Houseknecht, D. W., and Pittman, E. D., eds., *Origin, Diagenesis, and Petrophysics of Clay Minerals in Sandstones: SEPM Special Publication no. 47*, Tulsa, Oklahoma, Society for Sedimentary Geology, p. 209-225.
- Worden, R. H., and Morad, S., 2000, Quartz cementation in oil field sandstones: a review of key controversies, *in* Worden, R. H., and Morad, S., eds., *Quartz Cementation in Sandstones: International Association of Sedimentologists Special Publication no. 29*, Oxford, United Kingdom, Blackwell Science, p. 1-20.
- Worden, R. H., and Morad, S., 2003, Clay minerals in sandstones: controls on formation, distribution and evolution, *in* Worden, R. H., and Morad, S., eds., *Clay Mineral Cements in Sandstones: International Association of Sedimentologists Special Publication no. 34*, Oxford, United Kingdom, Blackwell Science, p. 3-41.

FIGURE CAPTIONS

Figure 1. Geologic map of the northern part of Valley of Fire State Park, modified from Flodin and Aydin (2004). WP: Waterpocket fault; BH: Bighorn fault; W: Wall fault; L: Lonewolf fault; C: Classic fault; M: Mouse's Tank fault; B: Baseline fault.

Figure 2. Map of diagenetic alteration units for area shown in Figure 1.

Figure 3. Photomicrographs (plain polarized light) of altered Aztec Sandstone. a. Hematite grain coat (arrow) in upper red unit. Pore space is partially cemented by kaolinite (k at top left of image). b. Patchy goethite grain coat (arrow) in yellow Aztec Sandstone. c. Hematite globules 5-10 μm in size in orange Aztec Sandstone. d. Goethite recrystallized to 1-3 μm sized grains (arrow) in purple band. e. White Aztec Sandstone is devoid of hematite grain coats. f. Pore-filling hematite adjacent to a joint.

Figure 4. Alteration of Aztec Sandstone at Valley of Fire. a. Boundary of lower red unit to overlying yellow unit at White Dome. Field of view about 0.5 km. b. Close-up of lower red boundary. Arrow points at layer of coarser hematite yielding a darker stain. c. Detail of lower red boundary at White Dome. Cusps (arrow) point toward yellow unit, lobes point toward lower red unit. Field of view about 50 m. d. Banded red and white unit. Basal conglomerate of Willow Tank Formation in background. Map case (30x40 cm, circled) for scale. e. White Aztec Sandstone (foreground) below allochthonous Aztec Sandstone of Willow Tank thrust sheet (background). Dashed line indicates position of thrust. Arrows point at bleached Aztec Sandstone along the base of the thrust sheet. The autochthonous and allochthonous sections of the Aztec Sandstone are separated by shale of the Willow Tank Formation (Kwt). Field of view about 0.5 km. f. Banded orange and white unit. Note alteration compartmentalization due to deformation bands. g. Banded orange and white unit crosscut by yellow and purple unit. Along contact, banded orange and white unit is altered to banded purple and white. Notebook (15x22 cm, circled) for scale. h. Boundary of white sandstone to upper red sandstone, cutting upsection across bedding. Banded red and white unit and basal conglomerate of Willow Tank Formation in background. Notebook (circled) for scale.

Figure 5. Crosscutting relations of alteration with faults and fractures. a. Lobes of orange unit with purple rim (arrows) extending into underlying white sandstone, preferentially following joints. Pocket knife (circle) is 9 cm long. b. Lobes of orange unit into white sandstone are offset

by 2-3 cm due to shear along joints 5-10 m west of the Bighorn fault (Fig. 1). c. Offset of the lower red to yellow boundary along the Mouse's Tank fault (Fig. 1), right side (E-side) away from viewer by 240 m of left-lateral strike-slip. Field of view about 40 m. d. Apparent offset of lower red to yellow boundary along compaction band. Offset is explained by relative retardation of alteration front on the left side of the deformation band. e. Preferred bleaching (arrows) of banded red and white unit along shear bands about 100 m south Willow Tank thrust. f. Bleaching of purple sandstone along joints. Field of view ~ 3 m. g. Tail of purple band around concretion (arrow) indicates direction of front advancement (in direction of arrow) to the SE and downsection. h. Kaolinite concretions preserved red stain due to preferred bleaching of surrounding sandstone. Kaolinite cemented layer (Fig. 2).

Figure 6. Schematic composite cross-section across diagenetic alteration units in Figure 2, based on field sketches taken from several vantage points. Due to the NW-ward plunge of the alteration units, the top parts of the section reflect observations in the northern portion of the map area, and lower parts are taken from observations in the southern portion of the map. Because alteration features do not project along strike over the extent of the map area this section represents an idealized composite. Although unit thicknesses and inclination are approximately to scale, horizontal distances are condensed to about half of the vertical scale.

Figure 7. Deflection of orange and purple bands along the Bighorn fault. a. Schematic cross-section. b. Kaolinite concretions along the fault (detail of a.) c. Purple-red stain along fault where in fault contact with the upper red sandstone (detail of a.). Map case (30x40 cm) for scale.

Figure 8. Stages of diagenetic alteration, fluid flow, and deformation in the Aztec Sandstone at Valley of Fire. a. Syndepositional reddening of eolian sandstone. b. First stage of bleaching and iron remobilization in upper section of the Aztec Sandstone associated with Sevier thrusting. Field observations suggest local flow along strike of the orogenic front but a regional direction of flow away from the orogen is inferred. c. Second stage of bleaching and iron remobilization associated with mixing of basinal and meteoric fluids during Basin and Range tectonics.

Figure 9. Schematic profile of fluid saturation relative to hematite as a function of distance across a coarsening reaction front or "side". On the upstream side of the reaction front, the reducing fluid is undersaturated relative to fine and coarse hematite causing dissolution of all hematite and bleaching of the sandstone. Within a transition zone, the fluid is undersaturated relative to fine hematite that gets dissolved but supersaturated for coarse crystalline hematite. Dissolution of fine hematite brings Fe into solution that leads to the growth of coarser crystalline hematite. Beyond the downstream side of the reaction front, the fluid is in meta-stable equilibrium relative to both coarse and fine hematite and no alteration reaction occurs. The thermodynamically favored replacement of fine hematite by coarse hematite is kinetically suppressed under these conditions.

Figure 10. $p\epsilon$ - pH diagram depicting the stability of iron oxides, iron hydroxides, sulfides, and sulfates in the presence of SO_4^{2-} and K^+ . Both hematite and goethite are shown as potentially stable phases. Jarosite and amorphous $Fe(OH)_3$ are shown for the absence of hematite, goethite, and magnetite, e.g. if due to kinetic reasons. Recalculated after Doner and Lynn (1989) using *Act2*, Release 4.0.2 (Bethke, 2002) and the "thermo.dat" data base. Solubility products for hematite and goethite after Trolard and Tardy (1987). Diagram is calculated for 80°C, 16 MPa, and activities of: $H_2O=1$, $Fe^{2+}=10^{-4}$, $SO_4^{2-}=5 \times 10^{-3}$, and $K^+=5 \times 10^{-4}$.

Figure 11. a. Compartments of sandstone formed by two sets of intersecting deformation bands resulting in systematic reddening and bleaching of sandstone adjacent to deformation bands and "ponding" of red stain next to the deformation band intersection. Coin (circled) for scale. b. Interpretation of a. Arrow indicates inferred flow direction of fluid. c. and d. Stereographic projections of deformation bands with associated alteration haloes for two locations A and B (Fig. 2) within the banded orange and white unit. Shading indicates deformation band compartments

that are bordered solely by bleached (blue) or reddened (red) faces. Compartments bordered by a combination of bleached and reddened faces are unfilled. Bedding reflects local orientation of cross-bedded strata. See text for interpretation of inferred flow directions.

TABLE 1. MINERALOGICAL COMPOSITION OF ALTERED AZTEC SANDSTONE

Sample #	Sample description	Location, longitude, latitude	qtz	K-fdspr	kaol	dick	smec	ill	I/S	R	hem	goe	alun	jar	other
04/04/01-3	red sndst in upper red unit	200 m E Bighorn fault 114° 31.47'W, 36° 29.09'N	x	x	-	x	-	-	90	3	xx	-	-	-	
04/04/01-5	white sndst below upper red unit	200 m E Bighorn fault 114° 31.47'W, 36° 29.09'N	x	x	x	-	-	-	90	3	-	-	-	-	
04/04/01-7	purple sndst in purple and yellow unit	200 m E Bighorn fault 114° 31.44'W, 36 °28.93'N	x	x	x	-	-	-	90	3	-	x	x	-	
04/05/01-4	yellow sndst	Fire Canyon Road 114° 30.34'W, 36° 27.25'N	x	x	x	-	-	-	90	3	-	x	-	-	
11/18/01-1C	hematite-stained sndst next to joint	Colorock quarry 114° 41.16'W, 36° 23.80'N	x	-	(x)	-	-	(x)	90	3	xx	x	-	-	calcite
11/18/01-5	yellow sndst	Buffington area 114° 41.14'W, 36° 23.13'N	x	(x)	-	-	-	-	90	3	-	xx	x	x	
11/20/01-1	orange sndst in banded orange and white unit	250 m E White Dome road 114° 31.51'W, 36° 28.55'N	x	-	x	-	(x)	-	90	3	(x)	-	x	-	
99-72	purple sndst	S White Dome 114° 31.98'W, 36° 29.00'N	x	-	x	-	-	-	90	3	-	x	x	x	
99-20	red sndst in lower red unit	S Mouse's Tank 114° 31.11'W, 36° 25.98'N	x	-	x	-	-	x	-	-	xx	x	-	-	(chlorite)
99-65	red sndst in lower red unit	S Rainbow Vista 114° 30.86'W, 36° 26.98'N	x	x	x	-	-	-	90	3	xx	(x)	-	-	

Note: qtz: quartz; K-fdspr: potassium-feldspar; kaol: kaolinite; dick: dickite; smec: smectite; ill: illite; I/S: illite/smectite mixed layer clay; R: Reichweite; hem: hematite; goe: goethite; alun: alunite; jar: jarosite; x...present, (x)... present in traces, -... below detection, xx... abundant (for hematite and goethite only).

TABLE DR1. ELEMENTAL COMPOSITION OF ALTERED AZTEC SANDSTONE

Sample #	Sample description	SiO ₂	Al ₂ O ₃	TiO ₂	Fe ₂ O ₃	MnO	CaO	MgO	K ₂ O	Na ₂ O	FeO
04/04/01-3	red sndst in upper red unit	94.43	2.46	0.043	0.21	0.002	0.04	0.13	1.43	0.21	0.09
04/04/01-5	white sndst below upper red unit	94.57	2.60	0.052	0.19	0.002	0.05	0.11	1.46	0.16	0.09
04/04/01-7	purple sndst in purple and yellow unit	94.73	2.48	0.039	0.04	0.002	0.04	0.12	1.35	0.22	0.26
04/05/01-4	yellow sndst	95.55	1.90	0.035	0.00	0.002	0.07	0.11	0.62	0.22	0.26
11/18/01-1C†	hematite-stained sndst next to joint	90.18	3.18	0.061	2.70	0.002	1.11	0.17	2.22	0.09	0.51
11/18/01-5	yellow sndst	93.05	2.26	0.039	0.72	0.000	0.05	0.08	1.34	0.26	0.26
11/20/01-1	orange sndst in banded orange and white unit	95.45	1.68	0.030	0.01	0.002	0.04	0.09	0.58	0.22	0.44
99/72	purple sndst	94.63	3.02	0.063	0.07	0.003	0.16	0.29	0.10	0.11	0.18
99/20	red sndst in lower red unit	93.65	3.12	0.105	0.24	0.005	0.08	0.17	1.46	0.19	0.17
99/65	red sndst in lower red unit	97.23	1.11	0.019	0.37	0.000	0.03	0.05	0.35	0.15	0.09
99/76	white sndst below upper red unit	96.31	1.78	0.040	0.00	0.002	0.04	0.09	0.92	0.11	0.18
99/76†		97.26	1.51	0.025	0.00	0.000	0.05	0.05	0.89	0.03	0.18
repeat†		97.24	1.50	0.025	0.00	0.000	0.05	0.08	0.88	0.03	

Note: All values in weight %. All samples by ICP-AES except † by X-ray fluorescence. FeO for all samples by titration.

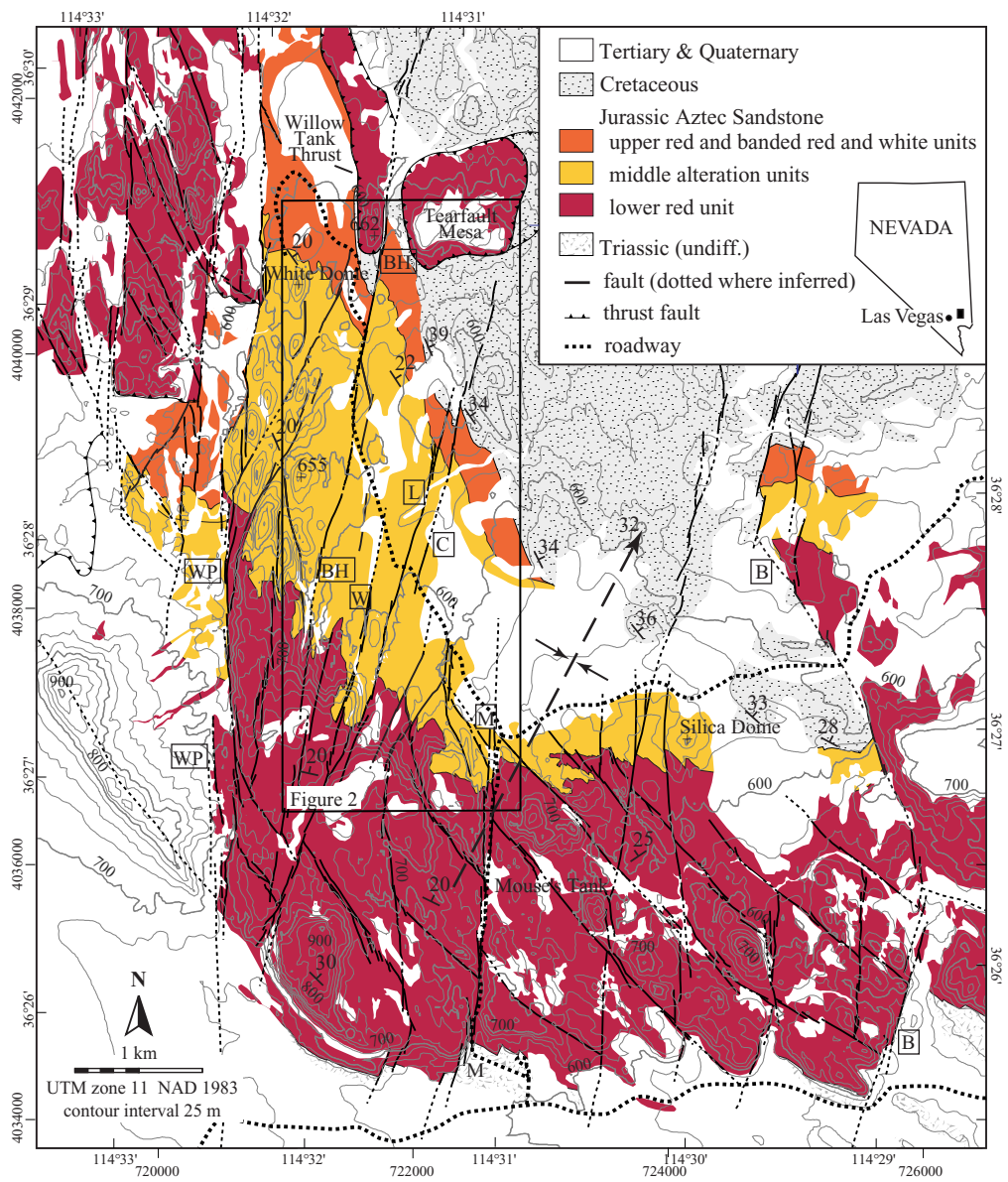


Figure 1.

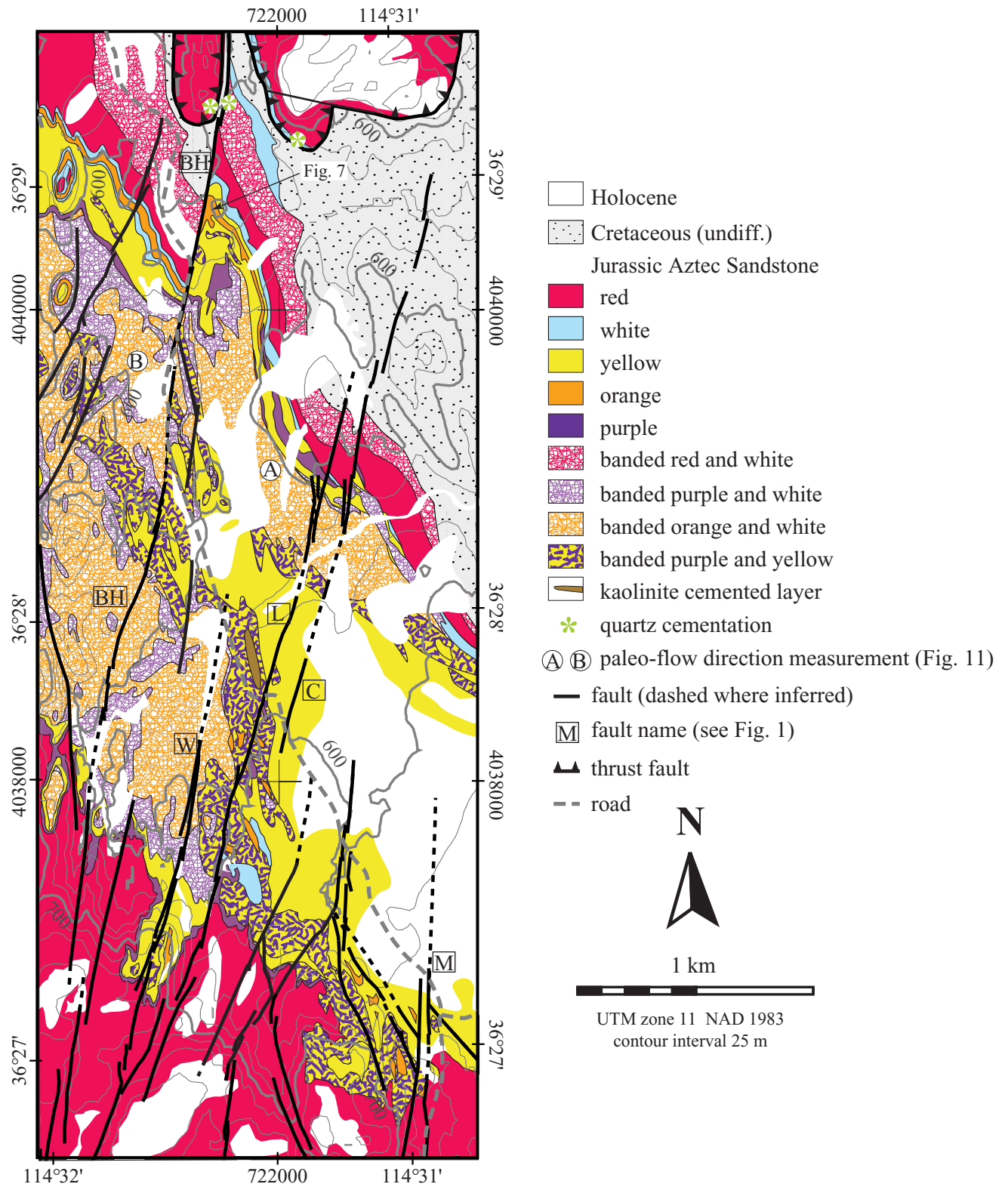


Figure 2.

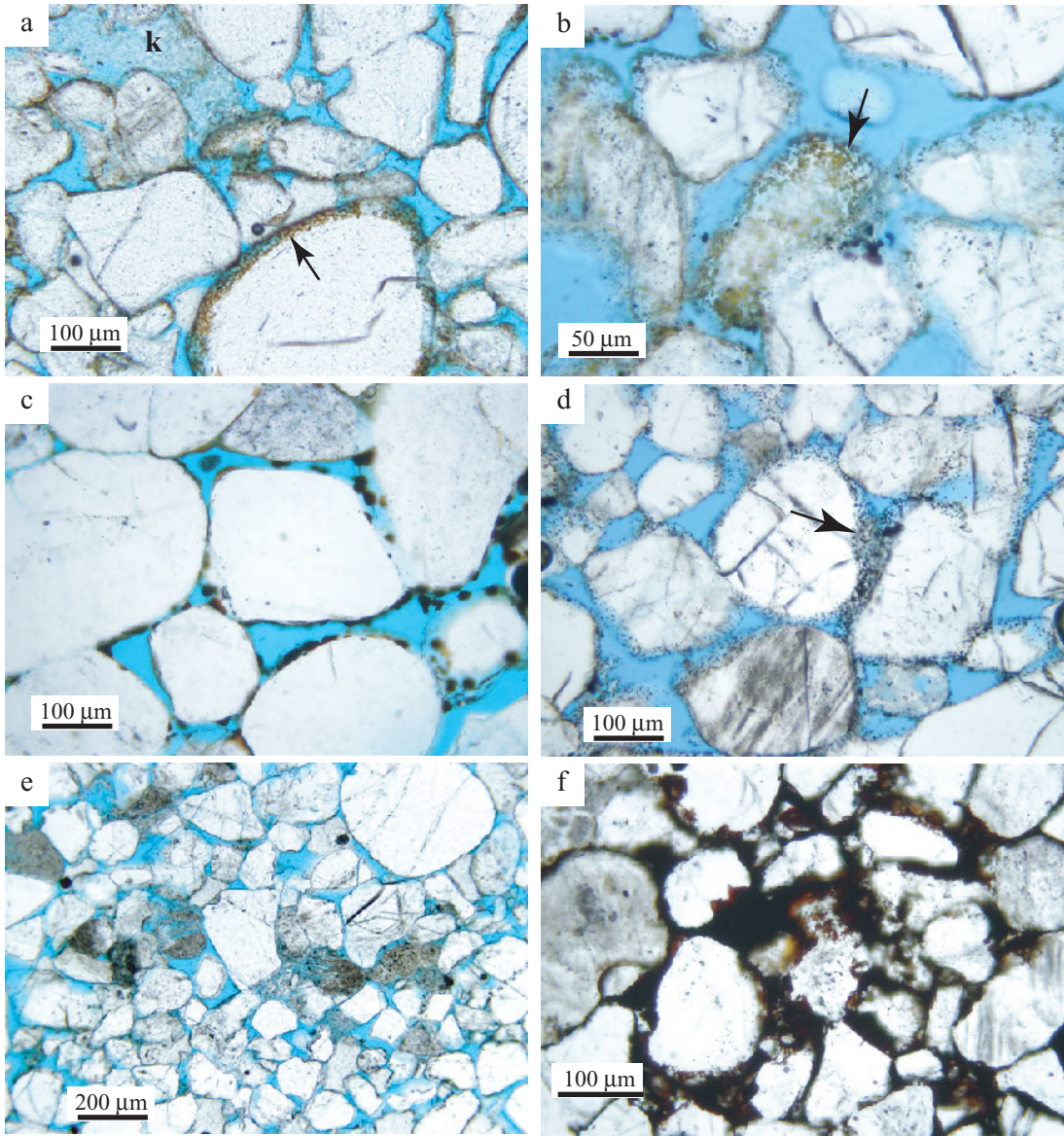


Figure 3.

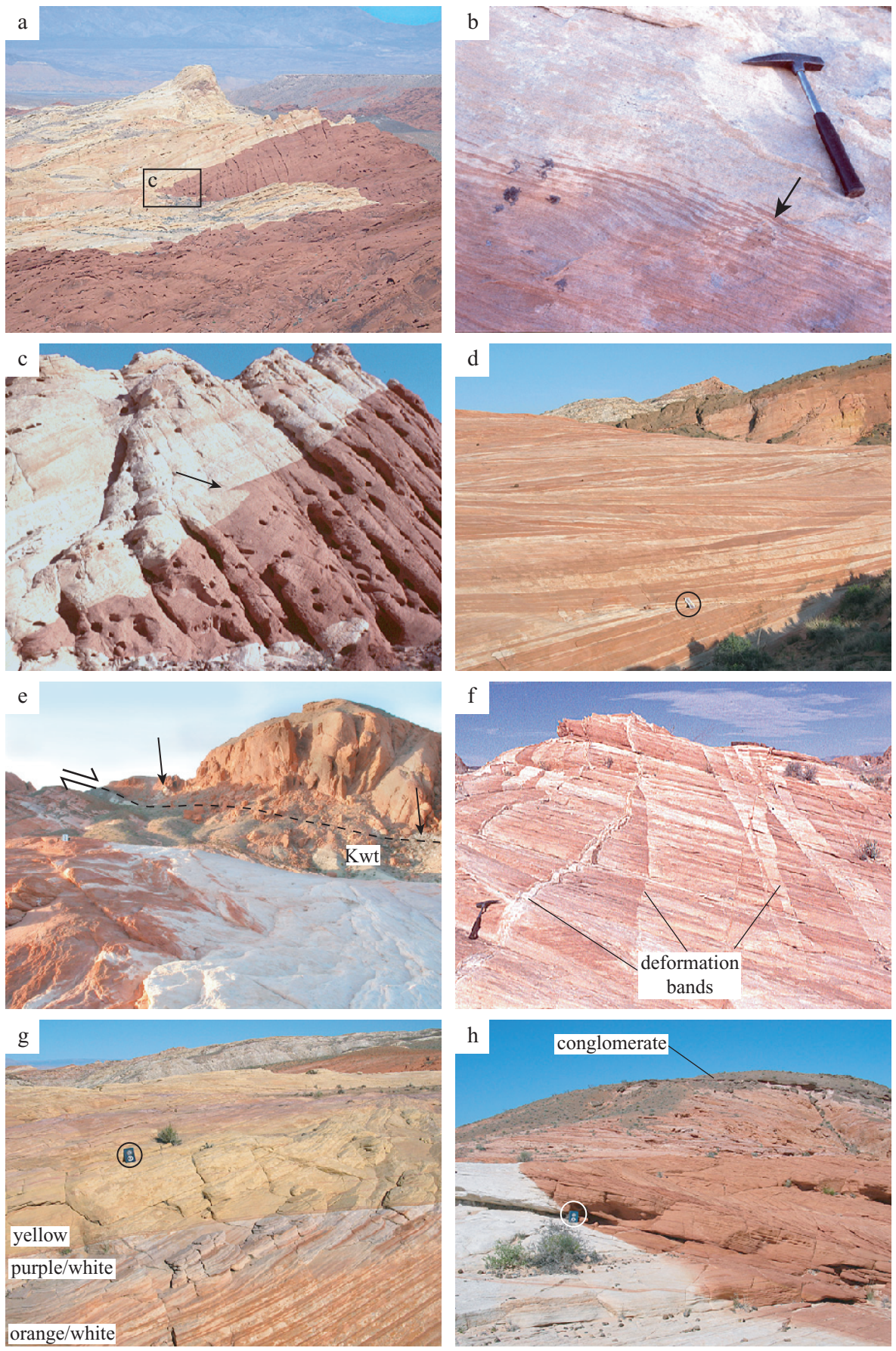


Figure 4.

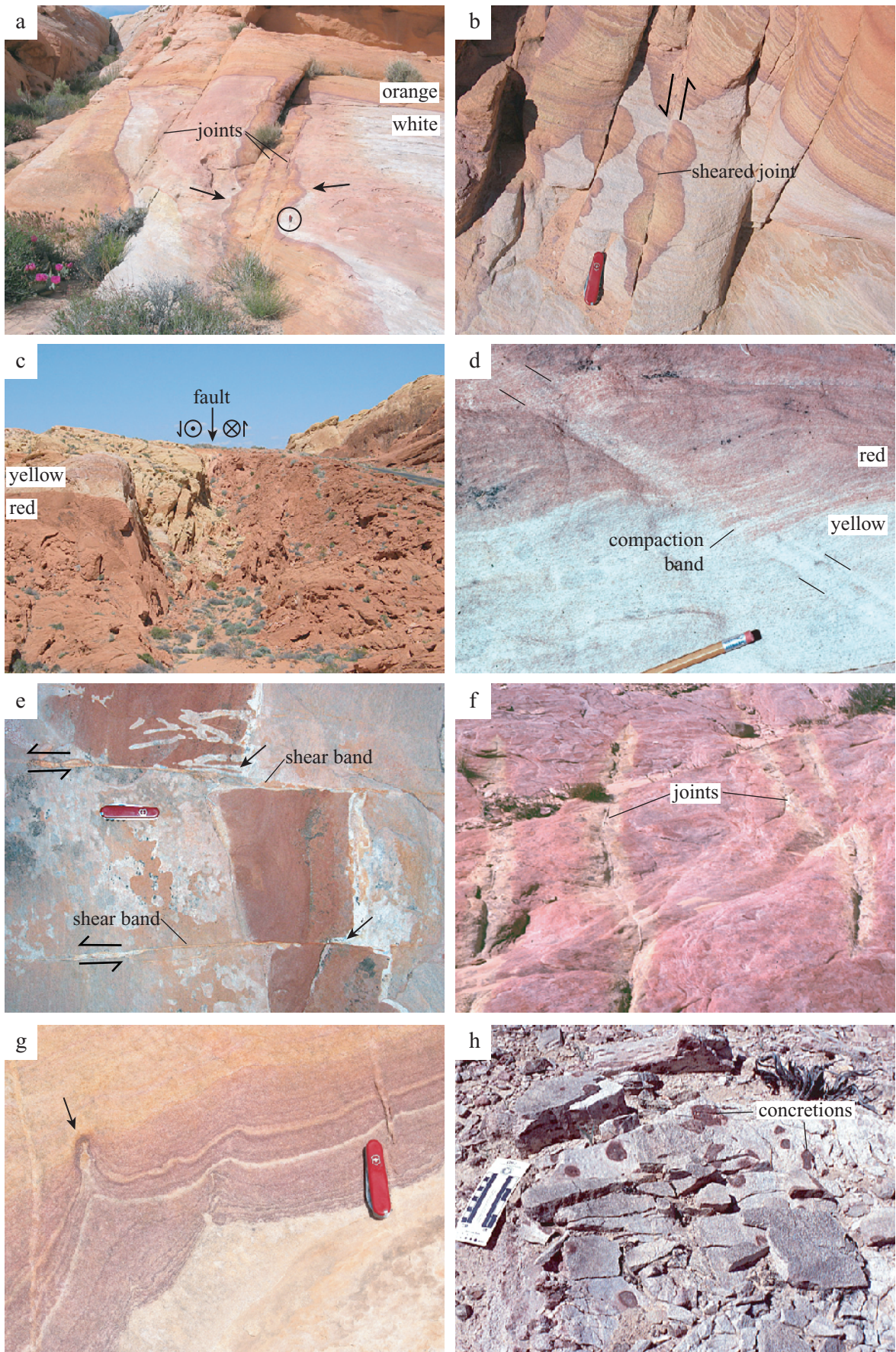


Figure 5.

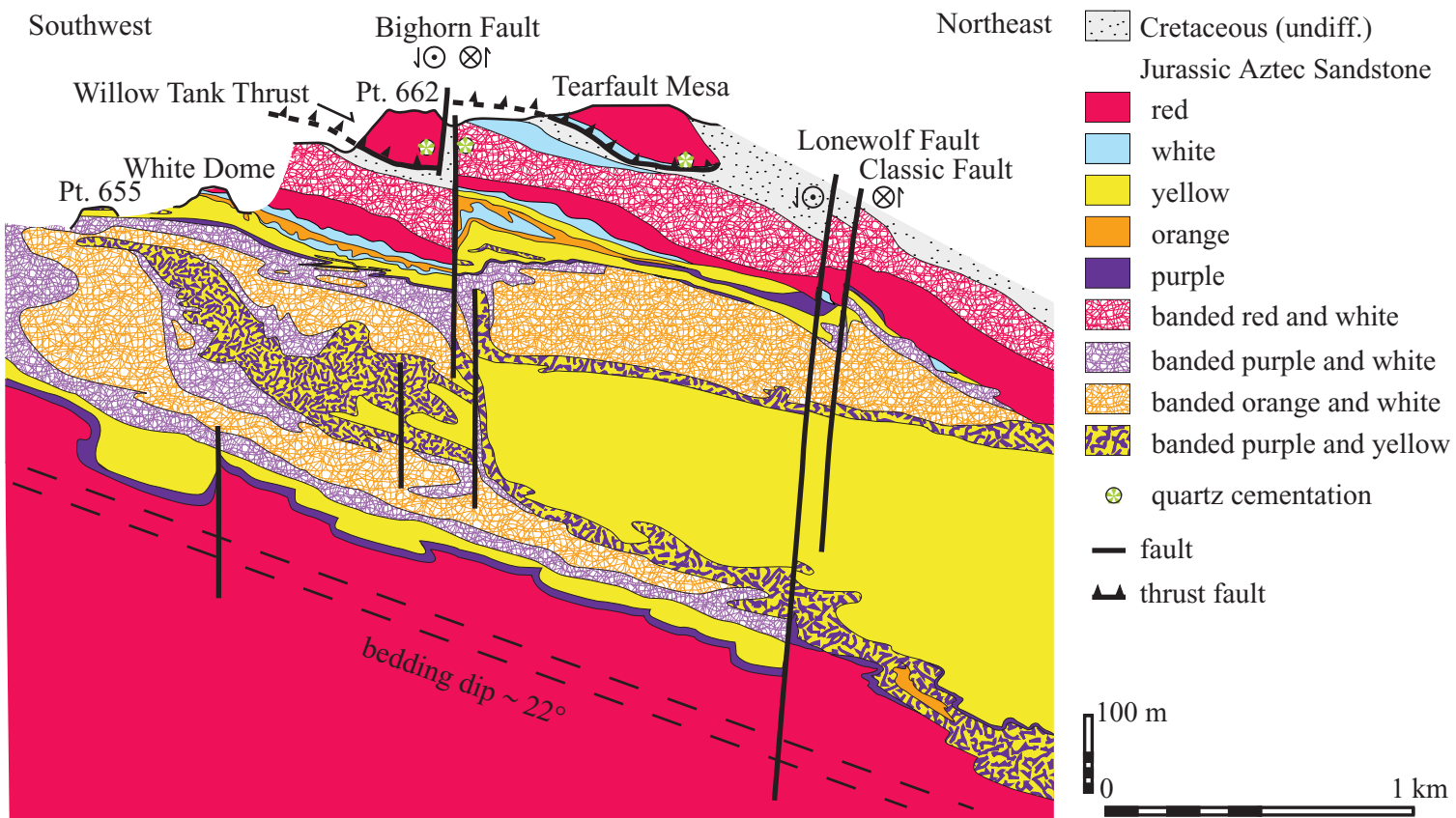


Figure 6.

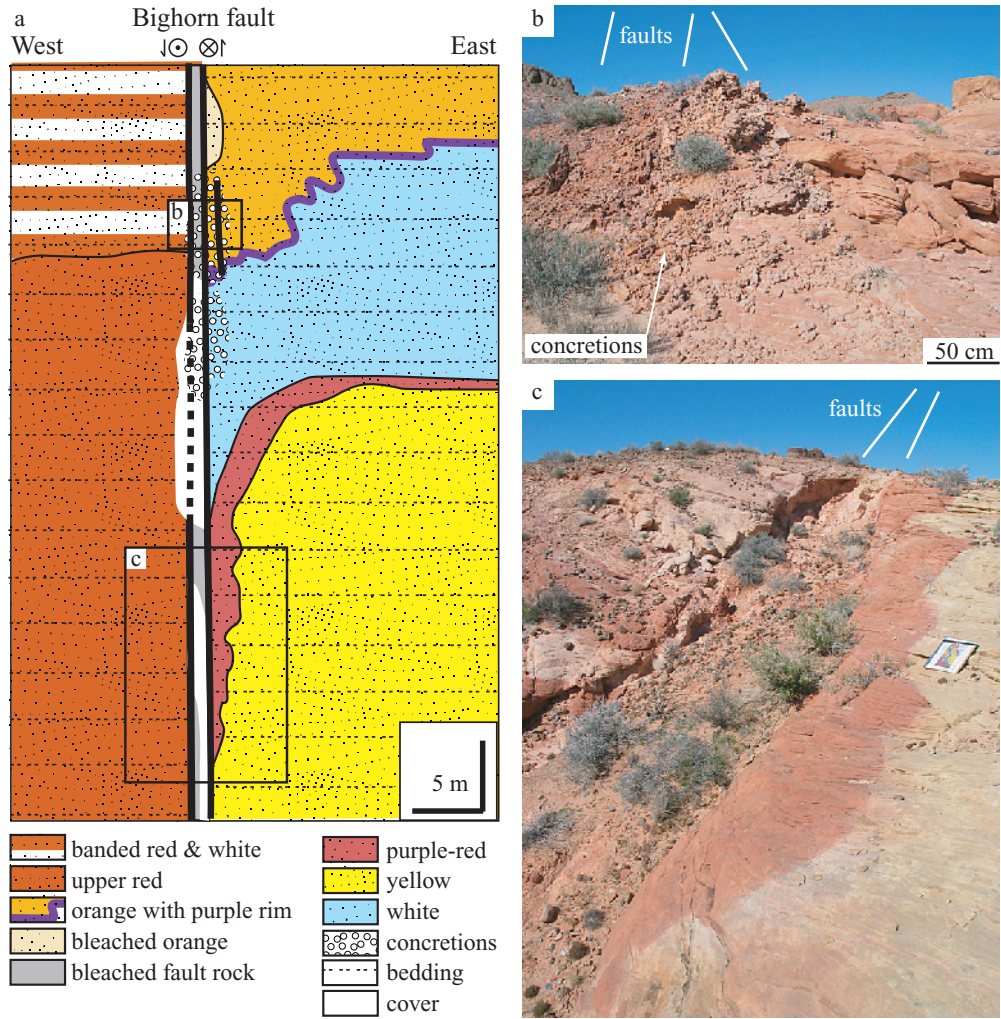


Figure 7.

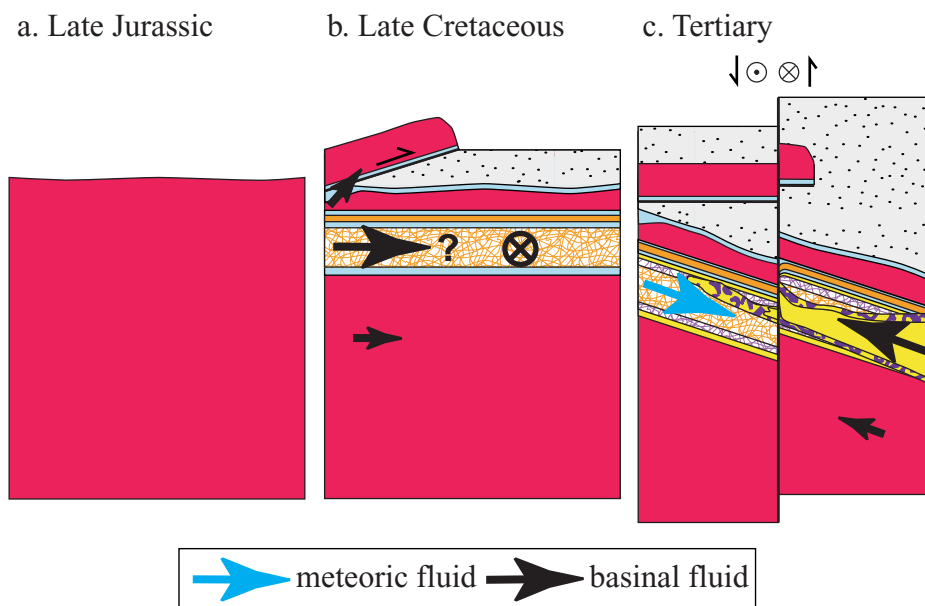


Figure 8.

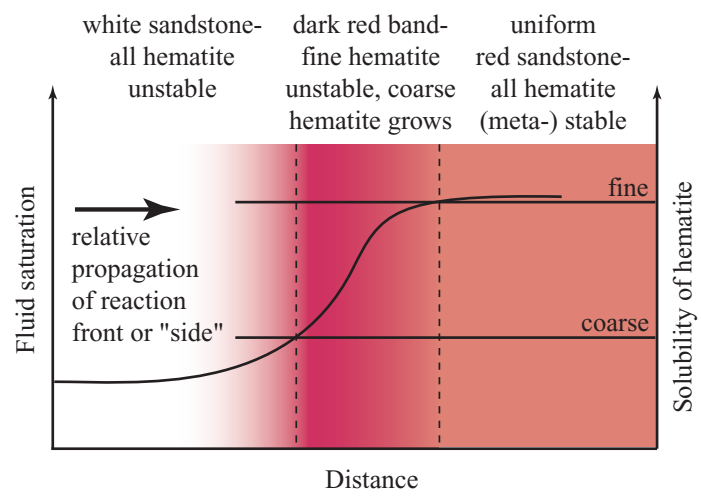


Figure 9.

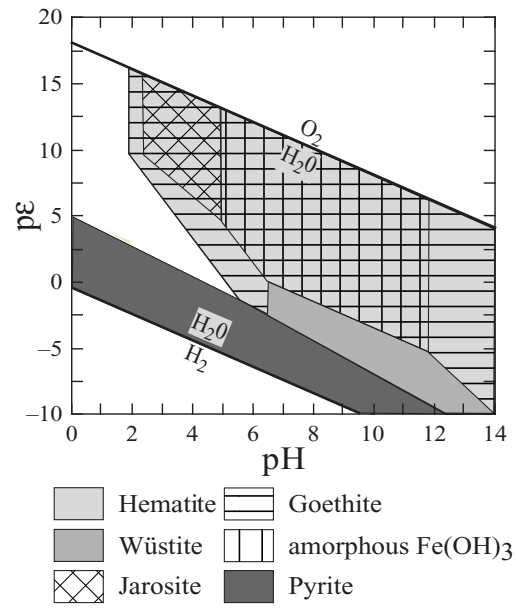


Figure 10.

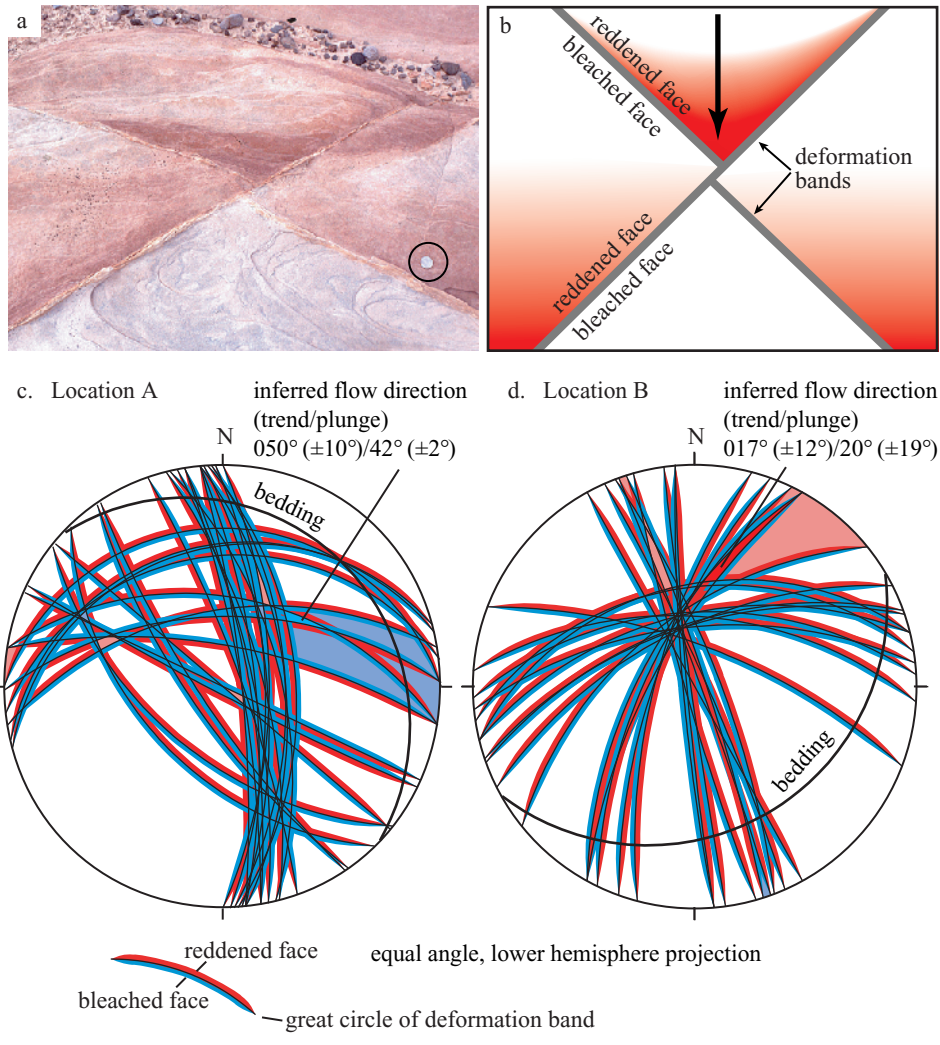


Figure 11.